CONTROLLING STRUCTURE BORNE NOISE IN AUTOMOBILES USING MAGNETORHEOLOGICAL COMPONENTS

by

Michael Henri Sjoerdsma
B.A.Sc., Simon Fraser University, 2002

THESIS
SUBMITTED IN PARTIAL FULFILLMENT OF
THE REQUIREMENTS FOR THE DEGREE OF

MASTER OF APPLIED SCIENCE

In the School
of
Engineering

SIMON FRASER UNIVERSITY

Spring 2005

APPROVAL

Name: **Michael Henri Sjoerdsma**

Degree: **Master of Applied Science**

Title of Thesis: **Controlling Structure Borne Noise in Automobiles using Magnetorheological Components**

Examining Committee:

Chair: **Dr. Karim Karim**
Assistant Professor,
School of Engineering Science, Simon Fraser University

Dr. Ash M. Parameswaran
Senior Supervisor
Professor,
School of Engineering Science, Simon Fraser University

Dr. Andrew Rawicz
Supervisor
Professor,
School of Engineering Science, Simon Fraser University

Dr. Shahram Payandeh
Internal Examiner
Professor,
School of Engineering Science, Simon Fraser University

Date Defended/Approved: April 15, 2005

SIMON FRASER UNIVERSITY

PARTIAL COPYRIGHT LICENCE

ABSTRACT

Car manufacturers are reducing the mass of automobiles in order to increase fuel efficiency. However, a lighter vehicle is more susceptible to structure borne noise, which can reduce a driver's safety due to fatigue. Magnetorheological components can semi-actively reduce structure borne noise.

This thesis describes two experiments: the fabrication of a bushing using magnetorheological fluid, and the creation of a magnetorheological elastomer using iron beads and silicone. The bushing had a negligible effect on the amplitude of the vibration except for a small change at the resonant frequency. The magnetorheological elastomer's resonant frequency changed significantly in the presence of a magnetic field. When the elastomer was cured within a magnetic field, so that the iron beads form chain-like structures, an even greater change in the modulus occurred. Additionally, results from further experiments show that the magnetic field orientation with respect to the direction of acceleration alters the magnetorheological effect.

DEDICATION

For my parents, Stan and Vicki Sjoerdsma.

ACKNOWLEDGEMENTS

I would like to thank my examining committee, Dr. Shahram Payandeh, Dr. Andrew Rawicz, and Dr. Ash Parameswaran. I especially thank Ash for all his guidance, support, and freedom he provides for his students. Thank you to Andrew for the use of his test equipment and his thought provoking questions and comments. I acknowledge the financial support of Auto 21.

Thank you to Nakul Verma for his help with research, car rides, editing and other Auto 21 related matters. Thank you to Ian Foulds for helping edit this document. Thanks to everyone else in Ash's research group for the interesting conversations regarding world matters.

A healthy mind needs a healthy body. Thank you to my friends at the Bog, the members of HFDC, and all those at SFU Hapkido.

I would like to thank my family, Vicki, Stan and Anne-Marie Sjoerdsma for all their support throughout my long academic career. Education begins early in life and I am grateful for the emphasis my parents placed on school in my childhood. Thank you to my friends Scott Kulchycki, Wes Wiens, Steve Duran, Yoon Choi, Steve Smyrl, Ted Lau, Justin Roberts, Olle Lagerquist, Alex Muir, and Brad Oldham.

Finally, I would like to thank my girlfriend, Lindsay Hindle, for all her support in the last two years. Meeting you was the best part of my Master's degree.

TABLE OF CONTENTS

LIST OF FIGURES

LIST OF TABLES

LIST OF EQUATIONS

LIST OF ACRONYMNS

ANC	Active Noise Control
ASAC	Active Structural Acoustic Control
DCM	Duty Cycle Modulated
EFC	Elastomer-ferromagnet Composite
ERF	Electrorheological Fluid
LVDT	Linear Variable Differential Transformer
mMRE	MRE cured in a magnetic field
MRC	Magnetorheological Components
MRE	Magnetorheological Elastomer
MRF	Magnetorheological Fluid
NCE	Networks Centres of Excellence
nMRE	MRE cured without a magnetic field
PCB	Printed Circuit Board
RMS	Root Mean Square

1 CONTROLLING STRUCTURE BORNE NOISE

1.1 Introduction

In order to increase the fuel efficiency of automobiles, car manufacturers are reducing the mass of their vehicles [1]. Unfortunately, lighter vehicles are more susceptible to structure-borne noise, which can reduce a driver's safety due to fatigue. Additionally, consumers associate a quiet automobile with quality and, therefore, car manufacturers have an economic incentive to make their automobiles quieter.

This thesis investigates methods for controlling structure-borne noise in automobiles. We describe two experiments using magnetorheological components (MRC). The first set of experiments involved creating a semi-active bushing using magnetorheological fluid. The second set of experiments involved creating magnetorheological elastomers to semi-actively control noise.

1.1.1 Auto21 Networks Centres of Excellence

Our research mandate was set forth by Auto 21, a Networks Centres of Excellence (NCE), consisting of various universities and industry sponsors from across Canada. Auto 21 is helping to create the automobile of the twenty-first century by investigating both the technical and social aspects of the automobile. The Auto 21 NCE has six research foci, which include: Health, Safety, and Injury Prevention; Societal Issues; Materials and Manufacturing; Powertrains, Fuels, and Emissions; Design Processes; and Intelligent Systems and Sensors.

Our research is under the Intelligent Systems and Sensors division in the team of Future Interior Noise. Additional information regarding Auto21 is located at www.auto21.ca.

1.1.2 Thesis Scope

We have divided the development of the MRC into three research modules: material development, electromagnetic control, and control algorithm.

Determining a viable means for attenuating structure-borne noise is the topic of this thesis. Our initial mandate was to investigate and implement a sensor/actuator for controlling noise in the cabin of an automobile. We investigated several techniques that can be used to control this noise. This thesis outlines the research that has lead to the conclusion that MRC can successfully attenuate structure borne noise.

Using the material developed in this thesis, the next research phase involves creating an electromagnetic circuit so that a variable magnetic field can be used to control the MRC. From these two modules of research, we will have a device that can control structure-borne noise in an automobile. The final stage of development will be to create a control algorithm for the component. This research module will include determining the appropriate sensors and their placement in the automobile, which will allow the development of a control algorithm.

1.2 Controlling Noise in Automobiles

The goal, when controlling noise in an automobile, is to create a quite cabin for the passenger. The noise produced in an automobile's cabin can have several sources, such as air-conditioning systems [2], engine noises [3], and noise from the road-tire interaction due to road roughness [4].

1.2.1 Active Noise Control

Theoretically, noise in the cabin of a car can be attenuated using Active Noise Control (ANC). This method uses the fundamental property that sound waves exhibit linearity at relatively low amplitudes and therefore superposition can be used to cancel noise [5]. Figure 1.1 illustrates a simple ANC system.

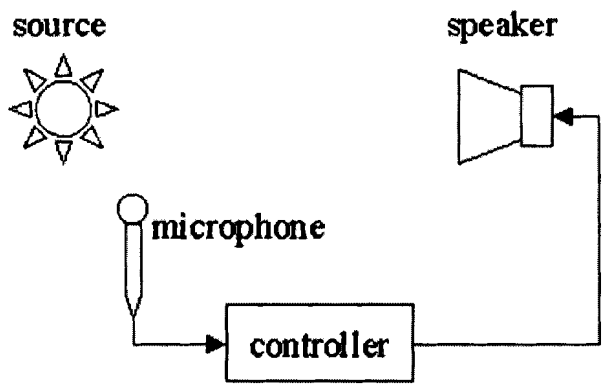

Figure 1.1: Simple ANC System

The microphone is placed near the source where the noise originates (closer to the source to maintain causality [6]). The signal, sensed by the microphone, is used as an input to a controller that changes the phase by 180 degrees and drives a speaker. Noise cancellation occurs near the speaker. This property of sound waves is easily illustrated with two sine

waves. If the waves have the same frequency and amplitude, but are 180 degrees out of phase, then the amplitude of the resultant wave will be zero as shown in Figure 1.2.

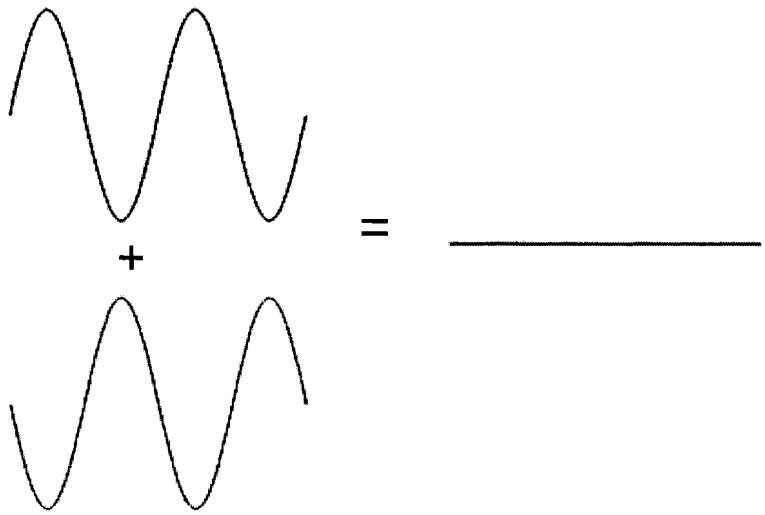

Figure 1.2: Destructive Interference of Two Sine Waves

These types of ANC systems are already used in headphone and headrest configurations to cancel noise [7], [8].

ANC is an attractive solution for controlling the noise in a car because passive techniques for controlling noise use absorbent material that has to be proportional to the wavelength being controlled. The audible frequency range for humans is between 20Hz to 20kHz. Recall that wavelength is equal to the speed of sound (330m/s at standard temperature and pressure) divided by the frequency, the wavelength for sound ranges from 17m to 17mm. For example, to damp 200Hz noise would require 2.5m of material [9]. Clearly, in the cabin of an automobile, this amount of material is impractical. Additionally, ANC is an attractive solution for controlling the noise in a vehicle because it does not introduce significant additional mass to the automobile [10], which is detrimental to increased fuel efficiency.

Although ANC has advantages over passive techniques, it has several limitations when applied to the cabin of an automobile. The main concern involving ANC is the number of sensors (microphones) and speakers needed to control the unwanted noise. The complexity of controlling all frequencies of audible sound occurs because sound in a small cavity is the result of standing waves, which are made up of a combination of modes. For the purposes of generality, let us assume that the cabin of an automobile has the following dimensions: 2 meters in length, 1 meter in height, and 1 meter width. For a cavity of these dimensions, the first longitudinal mode is 85Hz. At 170Hz, a problem arises because the attempt to cancel noise at this frequency will increase the noise associated with other modes. The excitation of other modes can be circumvented by using more microphones and speakers which are placed closer together. However, to accomplish active noise control at all frequencies up to 1kHz in such an enclosure would require 200 loud speakers [11]. Therefore, the use of ANC should be limited to frequencies no higher than 500 Hz [10].

S. J. Elliott and P. A. Nelson [12] have implemented a simple ANC system using eight microphones, six loud speakers, and a reference signal taken from the engine to control noise in an automobile. One major concern involving ANC is what noise to cancel out. A driver may want to listen to the radio or talk with occupants of the vehicle. If ANC is to be implemented it must accommodate these situations.

1.2.2 Active Structural Acoustic Control

Active structural acoustic control (ASAC) is similar to ANC except that the structure of the device is controlled instead of the sound waves inside of it. R. Cabell, D. Palumbo, and J. Vipperman [13] controlled the noise in the fuselage of an aircraft using

32 microphones and 21 inertial control actuators attached to the frame of an airplane. Instead of microphones and speakers, vibration sensing is accomplished with the use of piezoelectric sensors and actuators [14].

1.3 Structure-borne Noise

As stated, one source of structure-borne noise in automobiles is vibration caused by road-tire interaction. As a car drives over the road, noise is transmitted through the suspension system into the cabin of the automobile. Controlling noise directly at the source is one solution for removing noise in the automobile.

To control the road-tire vibration the suspension of an automobile must be modified. Commercially available automobiles have passive suspension systems. Modifications to the suspension can be either active, or semi-active.

1.3.1 Passive Suspensions

The suspension of an automobile has several functions which include: maintaining road-tire contact; enhancing handling performance; and minimizing forces to the occupants of the vehicle [15]. The majority of consumer vehicles have passive suspension systems consisting of springs and dampers. The major limitation of an automobile's suspension is that a trade-off exists between ride quality and handling [16]. That is, a passive car suspension cannot deliver optimal ride comfort while still delivering optimal handling performance. Because of this fact, passive suspensions must reach a compromise between these two opposing criteria.

A passive suspension system consists of springs and dampers (commonly referred as shock absorbers in automobile nomenclature). In order to model the behaviour of a

suspension, a quarter car model is used to represent the fundamental components of the system as shown in Figure 1.3. The quarter car model is used to analyze a car with respect to one of the wheels. This method is accurate for certain simulations, however, the entire car may have to be considered if elements such as roll are to be considered.

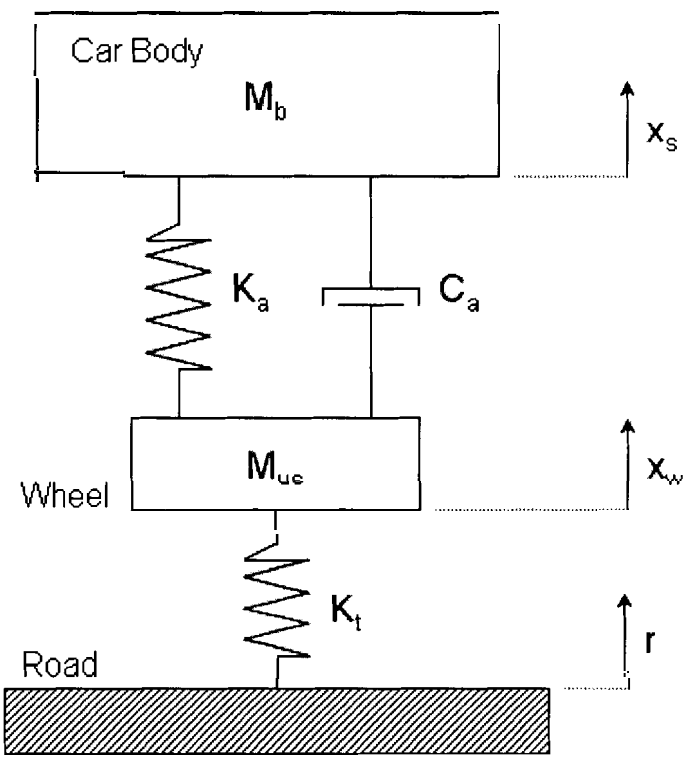

Figure 1.3: Quarter Car Model

The parameters for this model are summarized in Table 1.1 with typical values taken from Lin et al. [16].

Table 1.1: Quarter Car Model Parameters

Symbol	Name	Typical Value
M_b	Mass of Car Body	290 kg
M_{us}	Mass of Wheel	59 kg
K_a	Spring Coefficient (Suspension)	16,812 N/m
K_t	Spring Coefficient (Tire)	190,000 N/m
C_a	Damper Coefficient	1,000 N/(m/sec)

The movement of this system is described by the following equations [17]:

$$M_b\ddot{x}_s + K_a(x_s - x_w) + C_a(\dot{x}_s - \dot{x}_w) = 0, \qquad \text{Equation 1.1}$$

$$M_{us}\ddot{x}_w + K_a(x_w - x_s) + C_a(\dot{x}_w - \dot{x}_s) + K_t(x_w - r) = 0. \qquad \text{Equation 1.2}$$

As stated in section 1.1, when the mass of the automobile is decreased, the vehicle is more susceptible to structure borne noise. Using Equation 1.1and Equation 1.2 the transfer function for the movement of the car body, M_b, to an input r is

$$\frac{x_s(s)}{r(s)} = \frac{C_a k_t s + k_a k_t}{M_b M_{us} s^4 + (C_a M_{us} + M_b C_a)s^3 + (M_b k_a + M_{us} k_a + M_b k_t)s^2 + C_a k_t s + k_a k_t}.$$

Equation 1.3

The impulse response for two systems, one with a car mass of 290kg and one with a car mass of 190kg, is plotted in Figure 1.4.

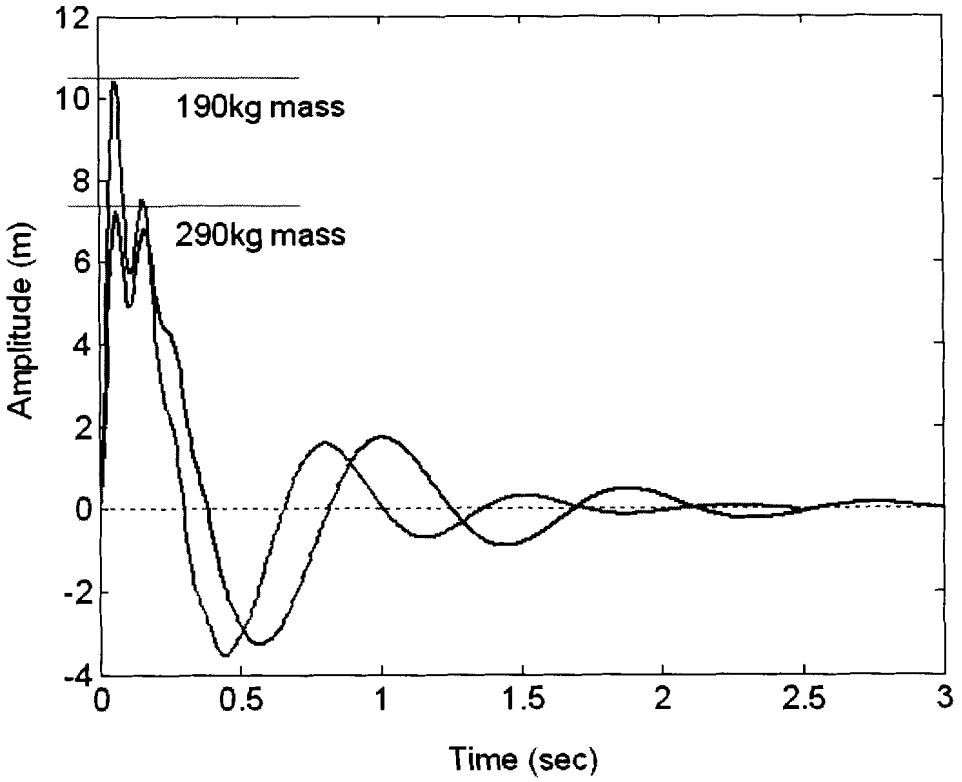

Figure 1.4: Impulse Response of Two Masses

The figure shows that the mass of 190kg has a greater amplitude than the mass of 290kg when subjected to the same impulse.

1.3.2 Active Suspensions

Active suspensions modify the typical passive suspension in an automobile by adding an actuator into the system. Depending where this actuator is added, the active suspension is either high or low bandwidth. Figure 1.5 illustrates a high and low bandwidth quarter car model.

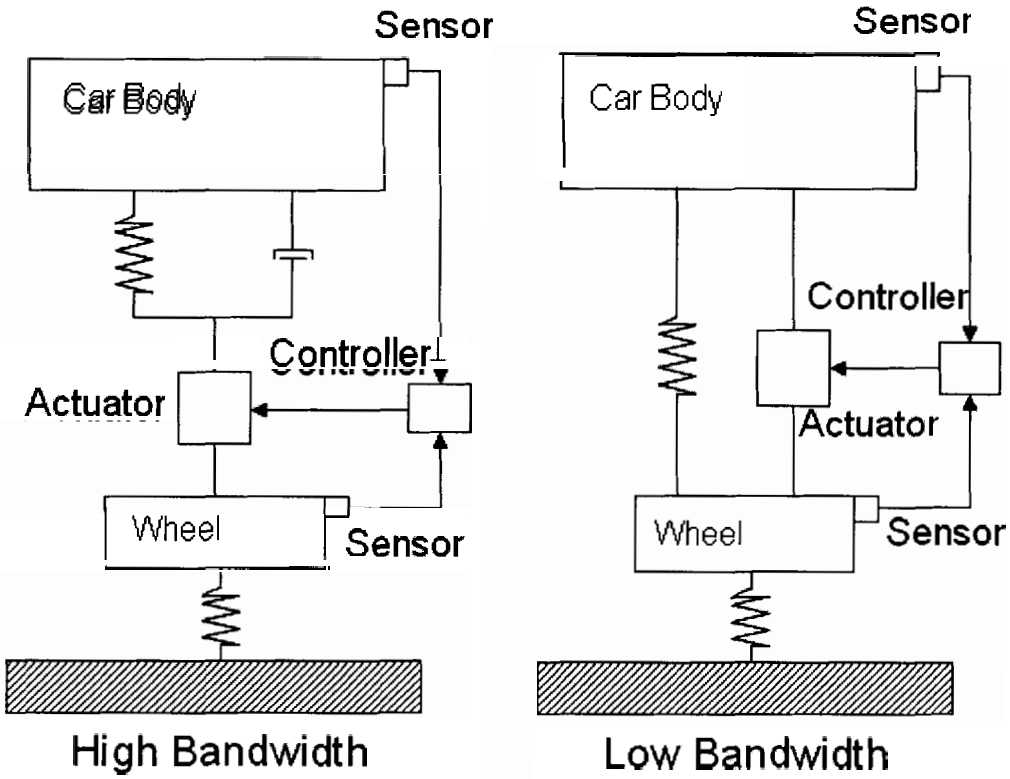

Figure 1.5: Quarter Car Model of Active Suspensions

In the high bandwidth system, the actuator is added in series with the existing spring and damper whereas, in the low bandwidth configuration, the actuator replaces the damper and is placed in parallel with the spring. William et al. [18] maintains that, because a high bandwidth system needs to control both the body and the unsprung mass (the wheel), aerospace technology is needed. Therefore, the low bandwidth configuration is more practical to implement in an automobile. Notice that in either configuration, the actuator is controlled by a control unit that uses strategically placed sensors as its inputs.

Although active suspensions have the ability to remove the inherent trade off associated with passive systems, they introduce other problems. Shoireshi et al. [1] outlines several design considerations for active control system. Complexity and power consumption are important aspects to consider if active suspension systems are to be

incorporated into commercially available vehicles [19], [20]. Additionally, because active components are used, the system has potential to become unstable if an inadequate control algorithm is used. Lin et al. [16] states that if the controller is designed to minimize force to the vehicle's occupants, to minimize body position, or to minimize the suspension travel then an unstable system or system with an oscillatory subsystem will result.

If an active suspension is used to control vibrational noise then the most important range for this system is between 0.5 Hz and 50 Hertz. Below the lower limit of this range, the car will track the road without introducing deflection in the suspension. Above the upper limit of this range, movement will be small in amplitude and outside the bandwidth of the suspension dynamics [21].

1.3.3 Semi-Active Suspensions

Similar to active suspensions, semi-active suspensions modify the traditional passive system. Instead of adding an actuator, a semi-active suspension replaces a passive damper with ones whose damping coefficient is variable. Semi-active suspensions have the benefits of active suspensions while minimizing power consumption [22]. Unlike active suspensions which may become unstable, semi-active systems are always stable because they do not introduce energy into the system; instead they vary how much energy the system absorbs [23], [24].

Research [25] has shown that a semi-active damper using electrorheological fluid can change the damping characteristics of a system. In 1985, Rakheja and Sankar [26] observed when the damping force was in the same direction as the spring force, the

acceleration of the mass increased. Therefore, a semi-active damper can control vibration by changing its damping force at the appropriate moment so that it does not cause an increase in the mass's acceleration. Theoretically, the damping force should be zero in the aforementioned situation. However, realistically achieving this damping force is difficult. Other control strategies have modified the Rakheja-Sankar control method [27].

1.4 Bushings

Another important element of a suspension that needs to be considered when discussing structure-borne noise in an automobile are bushings. Bushings are used in vehicles wherever the suspension meets the chassis of the automobile [28], as shown in Figure 1.6.

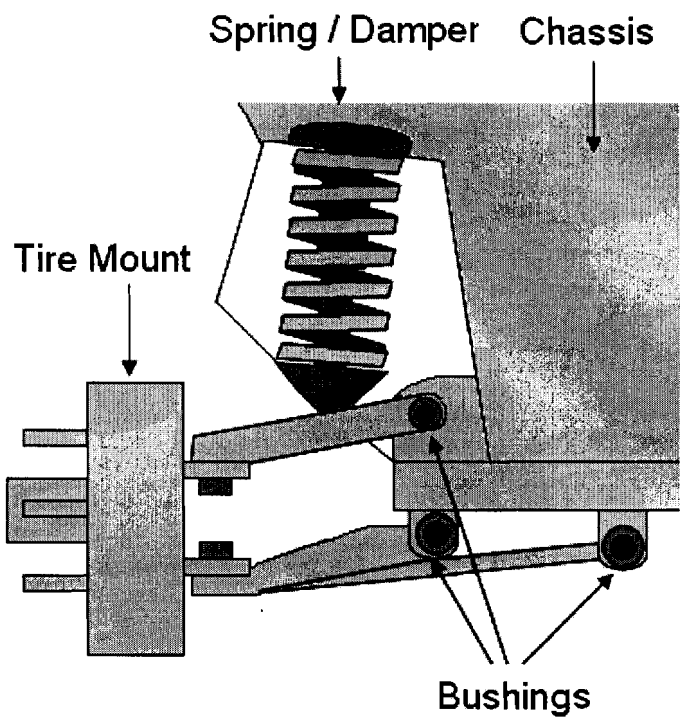

Figure 1.6: Bushings in a Suspension

Similar to the tradeoff found in a passive suspension, bushings compromise between reducing vibration transmission and handling performance. Commercially available cars have bushings made from rubber that limit unwanted noise while introducing play into the suspension system.

Many car enthusiasts replace the stock bushings that come with their automobile with polyurethane bushings that increase the handling performance of the automobile. While these custom bushings improve handling, they also subject the occupants of the vehicle to increased vibration.

Douville [29] has shown that structural noise is transmitted through the bushing. Even if an active or semi-active suspension is implemented in an automobile, unwanted noise will still transmit through the bushings.

Chapter 2 summarizes our experiments creating a semi-active bushing to attenuate the noise transmitted through this path in the suspension system.

2 A SEMI-ACTIVE BUSHING USING MAGNETORHEOLOGICAL FLUID

This chapter describes the development of a semi-active bushing using magnetorheological fluid (MRF). The ultimate goal is to incorporate a semi-active bushing into the suspension system of an automobile. The properties of magnetorheological fluids are discussed followed by a description of our test setup and experimental results. The work accomplished in these experiments was integral in the development of our final material, which we discuss in Chapter 3.

2.1 Magnetorheologocal Fluids and Electrorheological Fluids

2.1.1 Theory of Operation

MRF are composed of soft iron particles, approximately twenty to forty percent by volume, suspended in water, glycol, mineral, or synthetic oil [30]. These particles are in the order of three to five microns in diameter, although oxides have been used for particles which have allowed the size to decrease to thirty nanometers [30]. MRF is useful for semi-active systems because, with the application of a magnetic field, the rheological properties of the material change [31], and the fluid will alter from a free flowing liquid to a thick gel like substance.

Electrorheological fluids (ERF) are similar to MRF except that their rheological properties change with the application of an electric field [32]. When a field is applied,

the particles in the medium will align. A pictorial representation of the particles aligning with the field is illustrated in Figure 2.1.

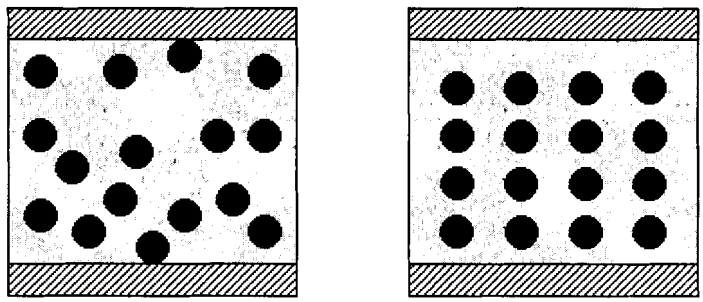

Figure 2.1: Rheological Fluid With and Without an Applied Field

When no field is applied, the particles in the fluid have no order and freely flow in the medium. However, when a field is applied, the particles align themselves with the field lines. This reconfiguration impedes the motion of the fluid thus increasing the viscosity. When the particles align with the magnetic field, the yield strength of the fluid increases, which is dependent on the field strength.

2.1.2 Current Applications

MR fluids were invented in the late 1940's by Rabinow, while Winslow was experimenting with ER fluids at approximately the same time. Initial concerns concerning rheological fluids involved sedimentation, abrasiveness and fluid durability [33]. With the improvements in rheological materials these concerns are no longer an issue. MRF have been used in several devices including rotary brakes in aerobic exercise machines, shock absorbers for NASCAR, forklift steer-by-wire systems, and prosthetic knee devices [33]. This list of applications of MRF shows that material can be used to

construct reliable, commercially available products and, therefore, is appropriate for implementing semi-active bushings.

2.1.3 Comparison Between ER and MR Fluids

As stated, both ERF and MRF fluids are substances that are able to change their rheological properties when an electric or magnetic field is applied, respectively. Theoretically, either of these fluids could be used to create a semi-active bushing. However, MRF are superiour to their ER fluid counterparts because they have a higher maximum yield stress, and are unaffected by most impurities [23]. Moreover, the power required for ERF is 2,000 – 5,000 volts at 1-10mA whereas MRF requires 2-50 volts at 1-10mA. Practically, ERF are unsuitable because the lowest operating temperature is –25 degrees Celsius [34] whereas MRF can operate in environments with temperatures as low as -40 degrees Celsius [23]. A semi-active bushing needs to work in climates that are below –25 degrees Celsius.

2.1.4 Modeling

Rheological fluids can be modeled using the Bingham plastic model where the total shear stress, τ, is defined as

$$\tau = \tau_0(H)\,\mathrm{sgn}(\dot{\gamma}) + \eta\dot{\gamma} \qquad \text{Equation 2.1}$$

where, τ_0 is the yield stress caused by an applied field H, $\dot{\gamma}$ is the shear strain rate, and η is the plastic viscosity. The shear stress versus strain rate is depicted in Figure 2.2.

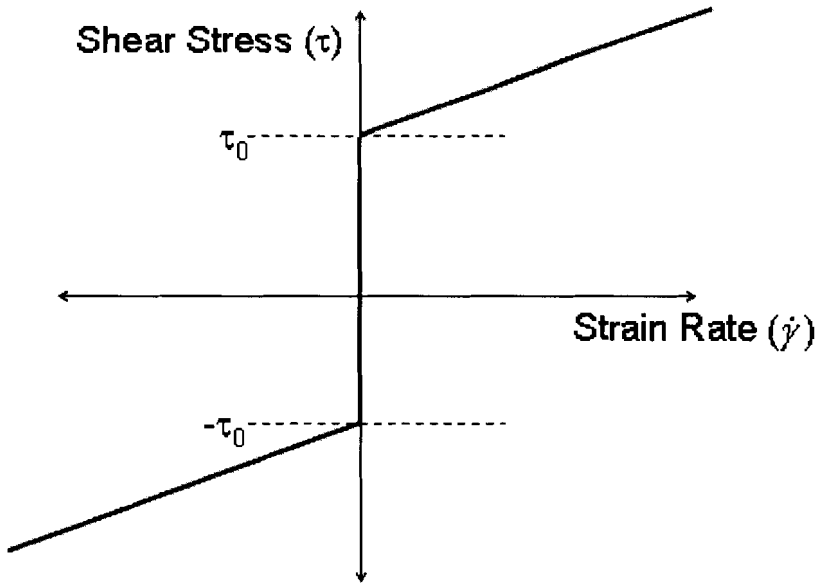

Figure 2.2: Shear Stress versus Strain Rate for a Bingham Fluid

This graph illustrates that the fluid will only flow once the critical shear stress, τ_0, has been reached [32]. Also note that in the Bingham model, the plastic viscosity is independent of field strength. The value for this term is calculated by the slope of the shear stress-strain rate curve. With this model, after the critical shear stress has been reached, the viscosity will be the same no matter the strain rate. In reality, the plastic viscosity changes for an MRF due to shear thinning effects. The Hershel-Bulkley model takes into account the shear thinning effects of the MRF.

In order to determine the modeling values for rheological fluids, Jolly et al. [31] have derived an excellent mathematical overview. They have determined that the rheological properties are dependent on particle size, particle density, and the shape distribution of the particles. Other techniques for modeling MRF have been explored by researchers [35], [36].

2.2 Semi-active Bushing Design

The semi-active bushing we constructed for our experiments was created from a modified Energy Suspension G.M. 4WD Front Spring Bushing (#2006) and a piece of machined hard rubber stock.

The inner diameter of the G.M. bushing was increased from 8mm to 33mm to accommodate the machined rubber, which had an outer diameter of 33mm. The rubber bushing was machined to have a bobbin like shape: the inner core having a length of 23.75mm and a diameter of 11mm with two wider ends with length 4mm and 6.95mm. The thicker end of this rubber structure has two 3.75mm in diameter holes on each side. Appendix A outlines the construction of the semi-active bushing in detail. Figure 2.3 summarizes the dimensions of the inner rubber bobbin.

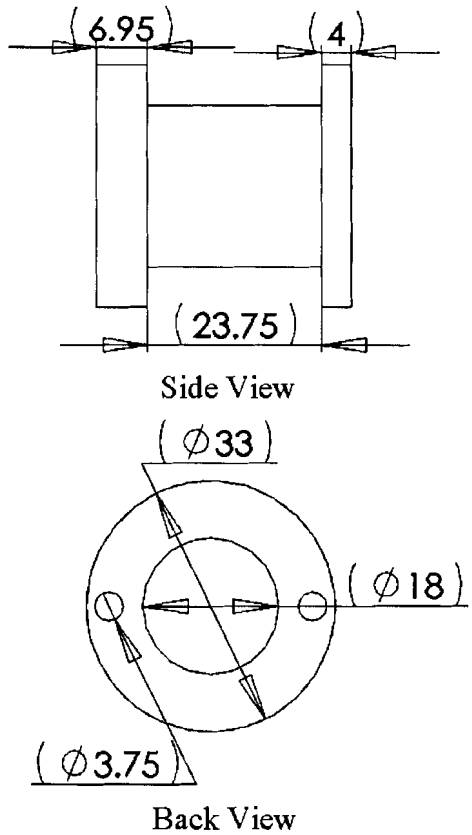

Figure 2.3: Inner Rubber Dimensions

We created a composite bushing using these two components, the G.M. bushing and the rubber stock, as well as three other sections introduced to the end of the bushing. After placing the rubber within the G.M. bushing sleeve, we affixed a polymer membrane over the end of the rubber core to seal the two holes. A neoprene core (approximately 5mm in length) was then sandwiched between the polymer membrane and a 3mm in length hard rubber end cap. An exploded view of the composite bushing is shown in Figure 2.4.

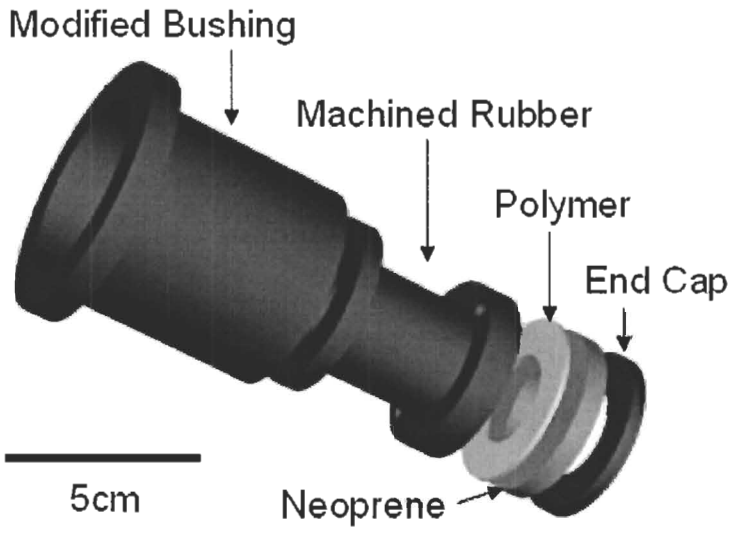

Figure 2.4: Exploded View of the Composite Bushing

Figure 2.5 shows the components used when constructing our semi-active bushing.

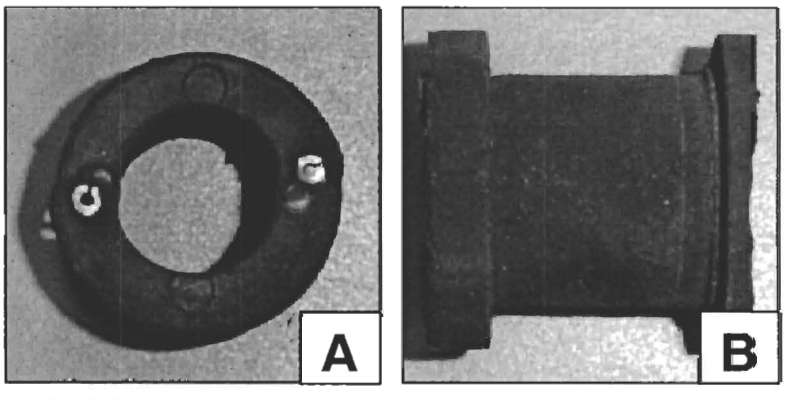

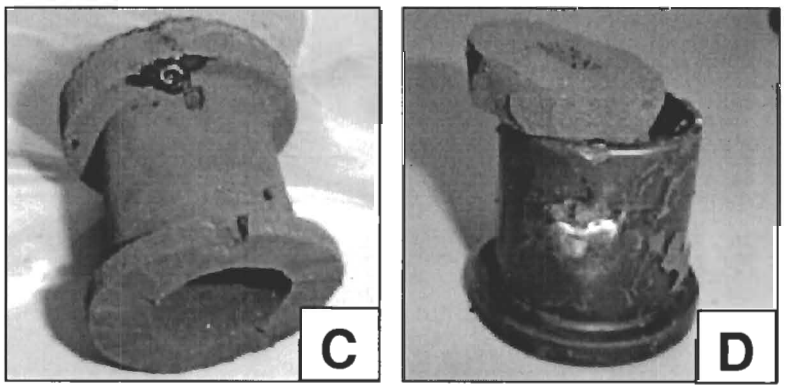

Figure 2.5: Various View of the Semi-active Bushing

Part A of Figure 2.5 shows a top view of the rubber bobbin with two holes to allow for the flow of the MRF. Part B of the figure shows the machined rubber bobbin from the side. Part C of the figure shows the rubber bushing with the polymer attached to the end. Part D of the figure shows the rubber bobbin in the outer sleeve with the neoprene about to be installed.

After assembling the bushing, as shown in Figure 2.5, we filled the cavity with Lord Corporation's MRF-122-2ED-8457-2 rheological fluid and placed the end cap to seal the entire device.

2.3 Theory of Operation

The volume flow rate, Q, of a fluid is described by

$$Q = \frac{\Delta P}{R}, \qquad \text{Equation 2.2}$$

where ΔP is a pressure difference and R is the fluidic resistance [37]. For laminar flow of a Newtonian fluid through a circular cross-section, R is defined as

$$R = \frac{8\mu L}{\pi r^4}, \qquad \text{Equation 2.3}$$

where μ is the viscosity of the fluid, L is the length of the channel, and r is the channel radius [37].

Our semi-active bushing changes the vibration transfer characteristics by altering the viscosity of the fluid passing through the end cap holes. With no magnetic field present, when the bushing is compressed, the MRF will pass through the end cap holes and press against the polymer membrane. The neoprene provides a restoring force that

will push the fluid back into the main cavity once the compression stops. When a magnetic field is present, MRF near the end holes aligns with the field lines and the pre-yield viscosity is infinite as shown in Figure 2.2. The bushing cannot compress because the fluid cannot move, which in turn causes the vibration to pass through the system.

A cross-sectional view of the side of a bushing is shown in Figure 2.6. The polymer, neoprene, and end-cap have been removed from the diagram.

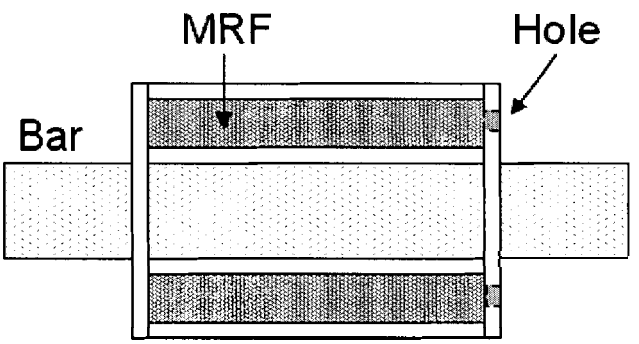

Figure 2.6: Side View of Semi-active Bushing

The MRF fills the entire cavity and when a force is exerted on the side of the bushing, the sides will press in causing the MRF to flow through the two side holes as shown in Figure 2.7.

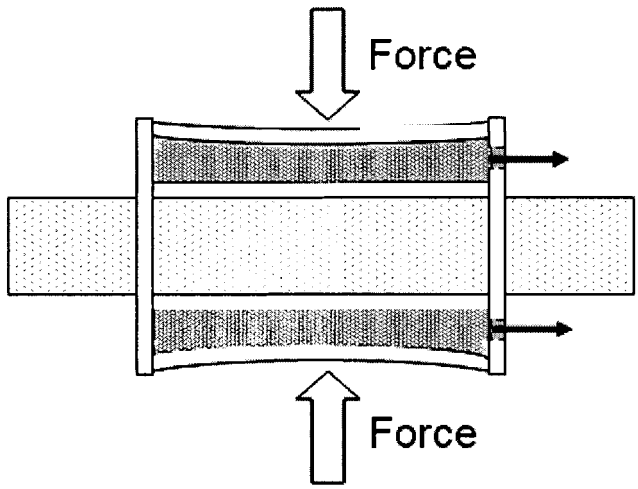

Figure 2.7: Bushing Compressed

If a magnetic field is present at the end holes of the bushing the fluidic resistance increases with the viscosity of the fluid as described by Equation 2.3. The fluid will not pass through the holes and, assuming that the compression of the MRF is negligible, the bushing will not damp any of the force.

2.4 Test Setup

We constructed a test rigging out of aluminum in order to conduct experiments using our semi-active bushing. Figure 2.8 shows our test setup.

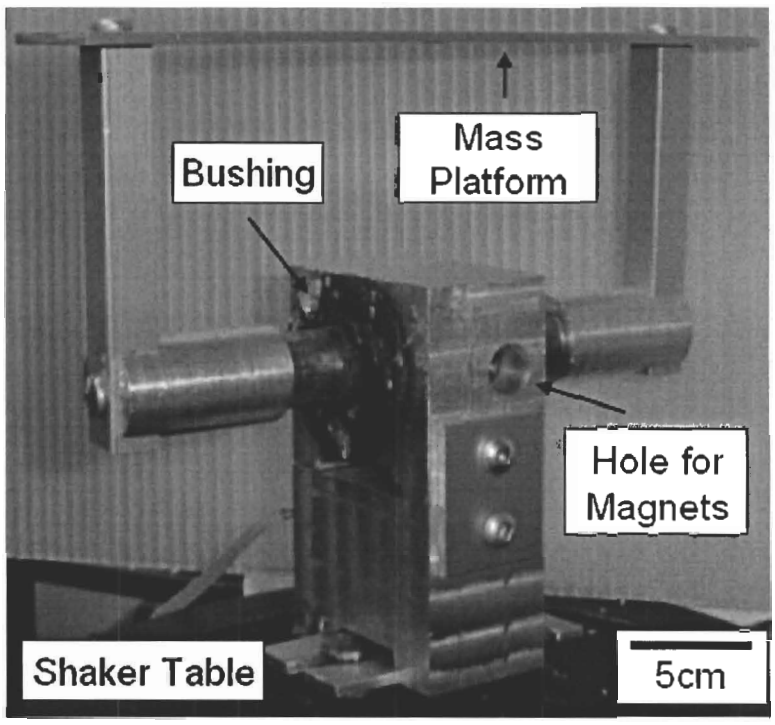

Figure 2.8: Test Setup

The bushing is placed within the aluminum block and has a metal rod placed inside of it. This rod is connected to a metal plate that allows the addition of mass to the system. The entire test rigging is fastened to a shaker table that provides the excitation vibration. Note, the test rigging is raised well above the shaker table to ensure that the magnetic field from the test equipment does not interfere with the MRF inside the bushing.

In order to determine the vibration transfer characteristics of the bushing, we used two Analog Devices ADXL210 accelerometers and an Atmel AT90S8515 AVR microcontroller. We attached one accelerometer to the bottom of the test rigging and the other accelerometer to the bar that is inside of the rubber bushing. The microcontroller determines the accelerations at each accelerometer by demodulating a pulse width modulated signal (see appendix A for more details).

To determine the transmissibility of the vibration transmission, we calculated the ratio of the bushings acceleration over the shaker table's acceleration with and without an applied magnetic field.

We excited the shaker table with a sinusoidal input that had an amplitude of 2 volts over a frequency range between 5Hz and 100Hz. We limited ourselves to the range because the most important range for an active suspension system is between 0.5 Hz and 50Hz. Below the lower limit of this range, the car will track the road without introducing deflection in the suspension. Above the upper limit of this range, movement will be small in amplitude and outside the bandwidth of the suspension dynamics [21].

We attached a 500g mass to the top of the test rigging. The magnetic field was applied using rare earth magnets. We measured the field strength of the magnets with a Group 3 DTM-133 Digital Teslameter 1mm away from the surface of the magnet. We measured a field strength of 0.25 Tesla. The magnets were placed inside the side holes in the aluminum block (see Figure 2.8).

2.5 Results

In general, over our tested frequency range, the semi-active bushing's vibration transmission was the same whether or not a magnetic field was present. The only variation we observed was between 69Hz to 71Hz. In this frequency range, the bushing gave an average transmissibility of 1.268. When we applied the magnetic field, the transmissibility was reduced to an average value of 1.139; giving a 10% reduction in the transmission of vibration when the magnets were introduced into the system.

2.6 Remarks

The results we obtained for our experiments were unexpected. The bushing only attenuated the vibration in a very narrow frequency range. The change we observed occurred at the resonance point of the system.

We have determined that these results occurred because the end caps of the bushing are too rigid and did not allow the bushing to compress. That is, the MRF is never being forced through the holes in the end of the bushing, which results in no difference when a magnetic field is provided. Figure 2.9 illustrates how the force is being transmitted through our bushing.

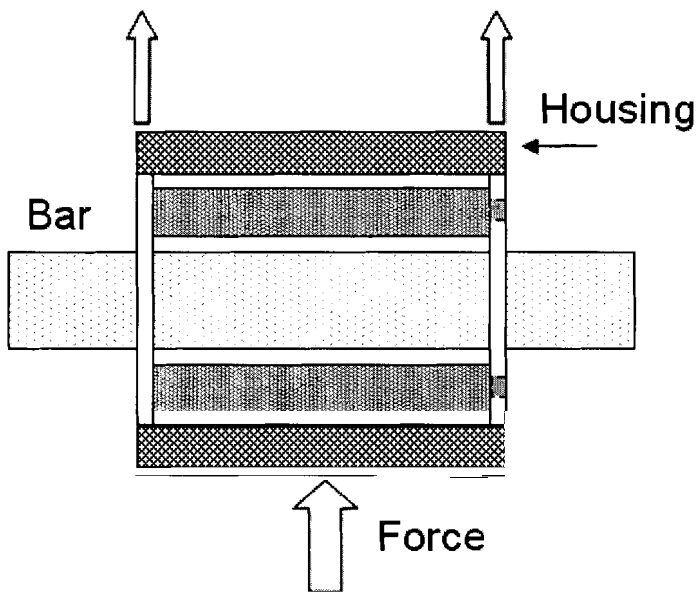

Figure 2.9: Bushing in the Test Housing

Figure 2.9, the housing represents the metal of the test structure and the force is from the shaker table. Because the end caps are too hard, they never compress, which never allows the cavity's shape to deform. If the cavity never deforms then the effect of the MRF is never realized. To circumvent this problem, we considered creating variable

end caps that would change their properties while in the presence of a magnetic field. On further investigation, we determined that having a cavity filled with MRF would be unnecessary; we could create the entire bushing out of the end cap material.

Our research showed that a smart material called magnetorheological elastomers could create such a device. We learned that a group from Ford [38] had already designed a semi-active bushing for an automobile. As a result, we decided to create our own elastomers to use for controlling other noise sources in an automobile, such as door panels and dash boards. Because of engine noise, door panels, windows, and other body panels vibrate [3]. Controlling vibration from these sources will reduce the amount of noise in the automobile's cabin.

Chapter 3 outlines the development of these elastomers.

3 MAGNETORHEOLOGICAL ELASTOMERS

3.1 Introduction

Magnetorheological elastomers (MRE) are similar to Magnetorheological Fluids (MRF) except that the particles are suspended in a solid matrix such as rubber or silicone rather than a liquid. MRE and MRF are not competing technologies because the former operates in the pre-yield range while the latter operates in the post-yield range [39]. MRE are used to change the natural frequency of a system by changing the stiffness of the structure [40]. Similar to MRF, the rheological change of an MRE occurs when a magnetic field is applied.

Iron particles are used to create MRE, although more expensive iron alloys of iron and cobalt or iron and nickel may be used [41]. Lokander and Stenberg [42], using various nitrile rubbers, experimentally determined that 30% iron particles by volume in the material results in the greatest rheological effect. Increasing the iron content in the MRE increases the stiffness of the composite material [43]. After the iron particles exceed 30% by volume, the increased stiffness of the composite exceeds the stiffness from an applied magnetic field [41].

3.2 Theory of Operation

3.2.1 Stress, Strain, and Elastic-modulus

When MRE are exposed to a magnetic field the elastic-modulus (also known as the Young's Modulus) of the compound changes. Recall that engineering stress is defined as

$$\sigma = \frac{F}{A_0}, \qquad \text{Equation 3.1}$$

where F is the force applied orthogonal to the cross section and A_0 is the cross-sectional area as shown in Figure 3.1.

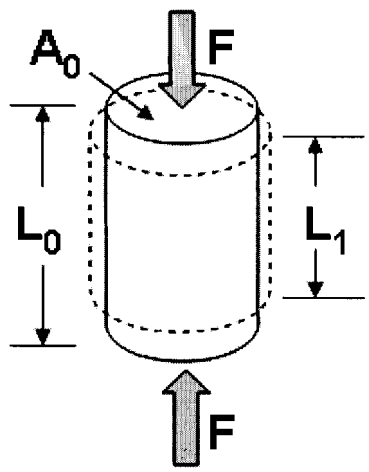

Figure 3.1: Dimensions Used for Stress and Strain

Engineering strain is defined as

$$\varepsilon = \frac{L_1 - L_0}{L_0}, \qquad \text{Equation 3.2}$$

where L_0 is the length of the material before a force F is applied and L_1 is the length once the force F is applied, as shown in Figure 3.1.

The Modulus of elasticity is defined as the ratio of Equation 3.1 over Equation 3.2, which yields

$$E = \frac{\sigma}{\varepsilon}, \qquad \text{Equation 3.3}$$

3.2.2 Modulus of Elasticity of a Magnetorheological Elastomer

The modulus of elasticity changes in an MRE when a magnetic field is applied [44]. To create an MRE, the elastomer is subject to a magnetic field which causes the particles to align. Once the elastomer has cured, the metal beads will remain in chain-like structures. Shen et al. [39], using these aligned chains, have calculated the MRE's shear modulus. Using dipole moment to model the MRE has been shown to be inaccurate. Borcea and Bruno [45] have derived the interaction of the particles for MRE with a random distribution within the matrix. They showed that the MRE elongates in the direction parallel to the applied magnetic field but, overall, compresses. Additionally, they showed that the strain perpendicular to the applied magnetic field is different from the strain parallel to the applied magnetic field.

3.3 Test Procedure

This section outlines our fabrication procedure for creating an MRE as well as the procedure we used to test its functionality.

3.3.1 Fabrication

To create the MRE, we used spherical iron powder (Alfa Aesar, stock #00736) with a mesh size of - 40+70 (45-70μm in diameter) for the suspended particles. For the matrix material, we used a silicone elastomer (Sylgard Brand 184). As discussed in

section 3.1, the optimum particle by volume percentage is 30% when the matrix material is nitrile rubber. Although our matrix material is silicone, we still used 30% iron particles by volume for our MRE.

We conducted preliminary tests where we tried to cure the iron beads in the silicone. We mixed the silicone elastomer base with the silicone curing agent and then we mixed in the iron beads. We observed that the beads settled due to gravity as shown in Figure 3.2.

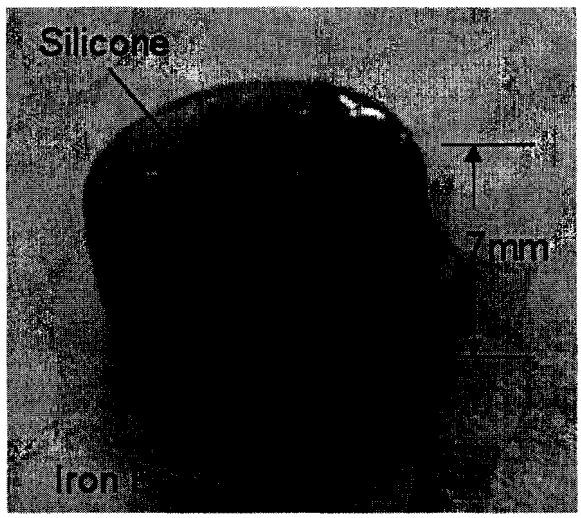

Figure 3.2: Iron Beads Settled in the Silicone Matrix

In order to avoid the beads settling, we mixed the base and curing agents together and let the silicone mixture become very viscous whereupon we mixed in the iron particles. Appendix C describes the fabrication procedure of the MRE in detail. We then poured this mixture into the mold shown in Figure 3.3.

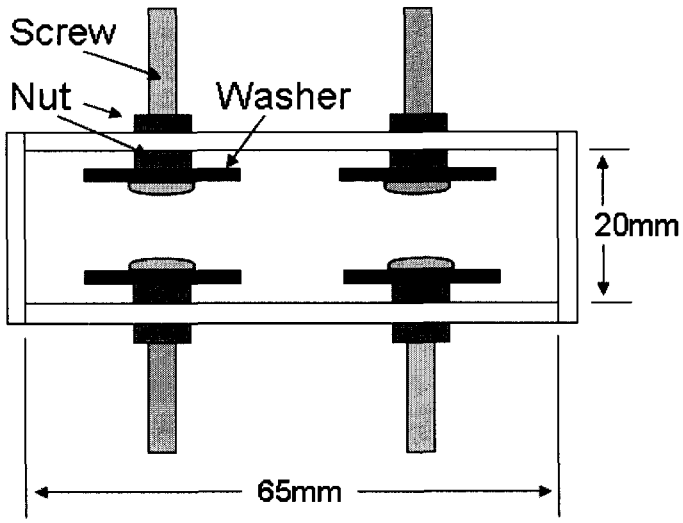

Figure 3.3: Top View of Silicone Mold

In Figure 3.3 the screws are used to secure the MRE to the test structure (refer to section 3.3.2). The washer and the nut inside the mold are used to secure the screw in place. The outer nut is removed after the curing process is completed and the outer shell is removed. Figure 3.4 illustrates the MRE after the molding process.

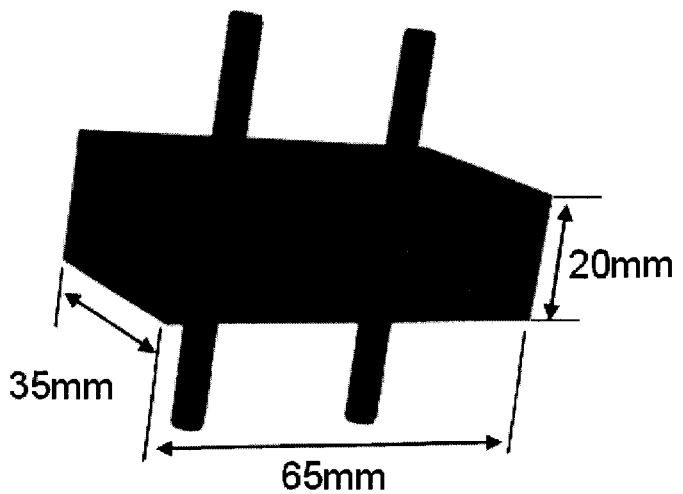

Figure 3.4: Fabricated MRE

3.3.2 Test Rigging

To test how the MRE changes when a magnetic field is applied, we used a procedure similar to Ginder et al. [38] where the MRE is excited using a sinusoidal input. Our experimental setup is illustrated in Figure 3.5

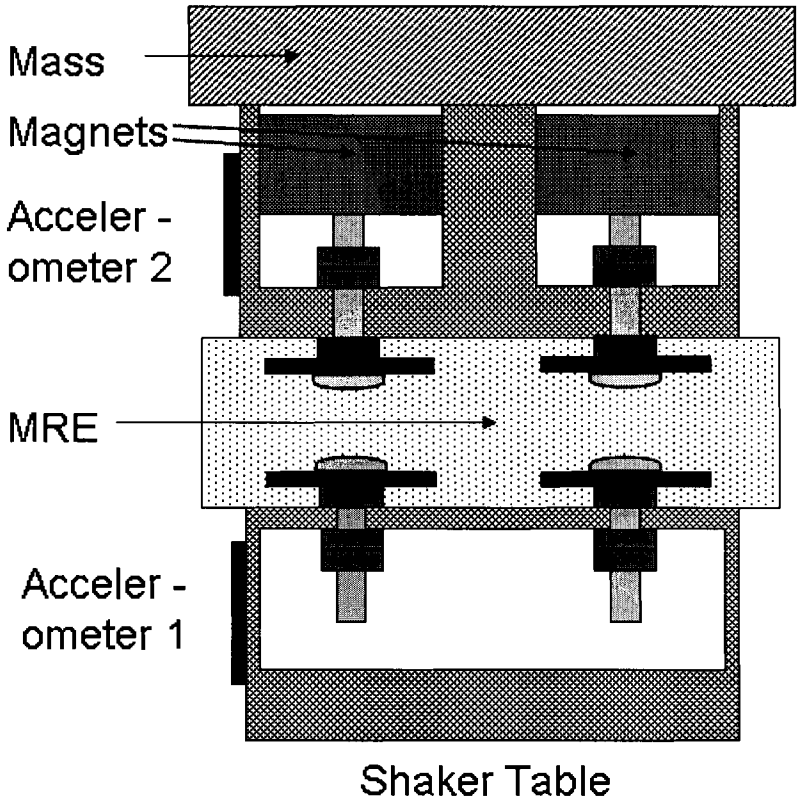

Figure 3.5: Cross Sectional View of the Experimental Setup

The MRE is attached to an aluminum base and an accelerometer (ADXL210) is used to ensure that the shaker table's acceleration remains constant. During preliminary tests, we discovered that the frequency response of the shaker table changed with frequency as shown in Figure 3.6.

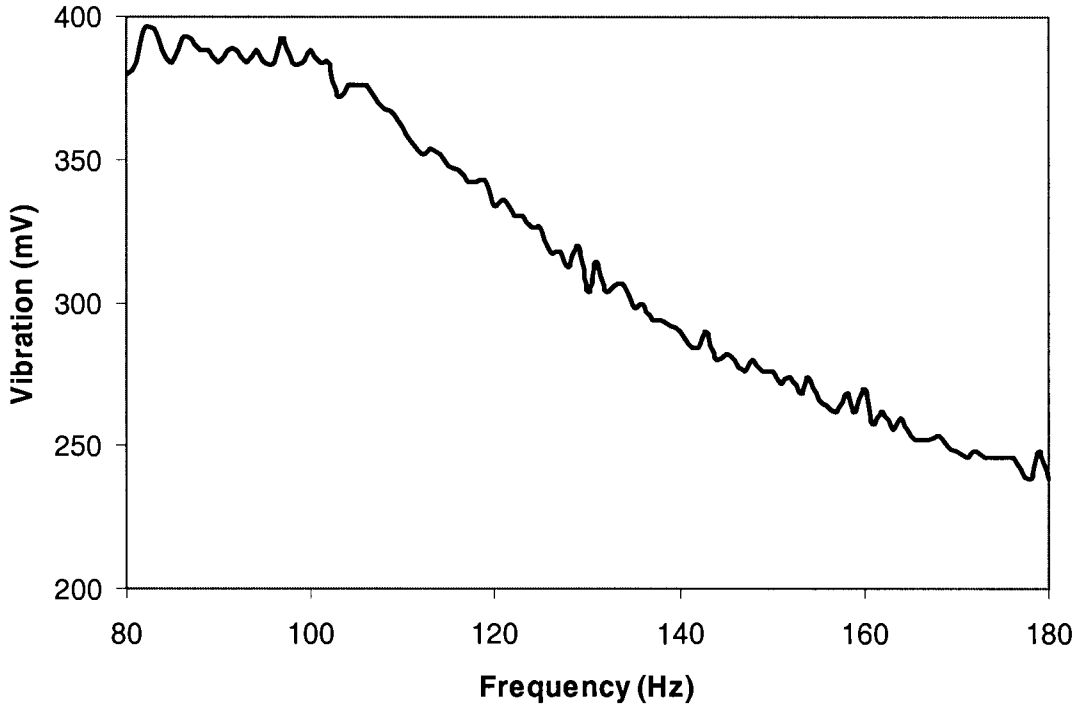

Figure 3.6: Shaker Table's Response

The y-axis in Figure 3.6 is the output voltage of the accelerometer. When we conducted our experiments we adjusted the gain so the shaker's output vibration remained constant.

The other side of the MRE is attached to an aluminum housing that can accommodate a permanent magnet. An accelerometer is attached to this housing.

3.4 Experimental Results

We fabricated and tested two versions of the MRE: the first version with the iron beads suspended in the silicone randomly, and the second version with the iron beads cured in a magnetic field so that they formed chain-like structures. When an elastomer is cured without an applied field, the resulting material is called an elastomer-ferromagnet composite (EFC) [46]. In this thesis, an elastomer cured with iron beads without an

magnetic field will be called an nMRE, and when cured with a field will be called an mMRE.

For the mMRE, we applied the magnetic field so that the chains formed perpendicular to the direction of acceleration as shown in Figure 3.7.

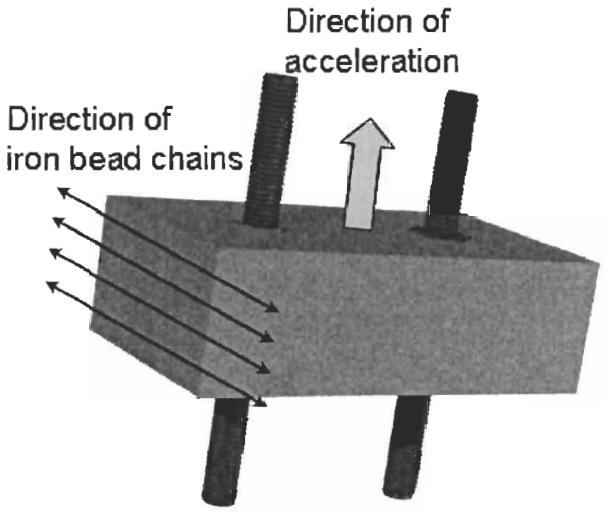

Figure 3.7: Direction of Iron Bead Chains

We chose to cure the beads in the direction of the width opposed to the direction of the length because the distance is shorter and we were more confident about the field lines. For our magnetic field we used four permanent magnets (Lee Valley 99K32.11 3/4''x 1/8''). Two magnets were placed on each side of the elastomer while it cured. The field strength at the magnets was 0.07T. Subsequent measurements showed that the field was only 0.03T in the center of the molding. A more uniform magnetic field will result in uniform chains forming in the elastomer.

For each MRE we tested the system with and without magnets. The field strength of the magnets 1mm from the surface was measured with a Hall Effect sensor and was found to be 0.258T. Each system was tested with three masses: 375g, 575g, and 675g.

When we removed the magnets from the system, we ensured that the overall mass of the system remained the same by adding additional weights to compensate for the magnets. For our testing, we used a 140mVp-p sine wave at frequencies between 15Hz and 215Hz. To calculate the transmissibility of the MRE, we took the ratio of the acceleration of the housing (accelerometer 2) over the acceleration of the base (accelerometer 1).

3.4.1 Experimental Results for the nMRE

The frequency response for the MRE cured with no magnetic field is shown in Figure 3.8, Figure 3.9, and Figure 3.10 for masses of 375g, 575, and 675g, respectively. Each graph contains a plot of the transmissibility versus frequency for the MRE with and without a magnetic field. The fractional change in resonant frequency (Δf) is labeled on each graph.

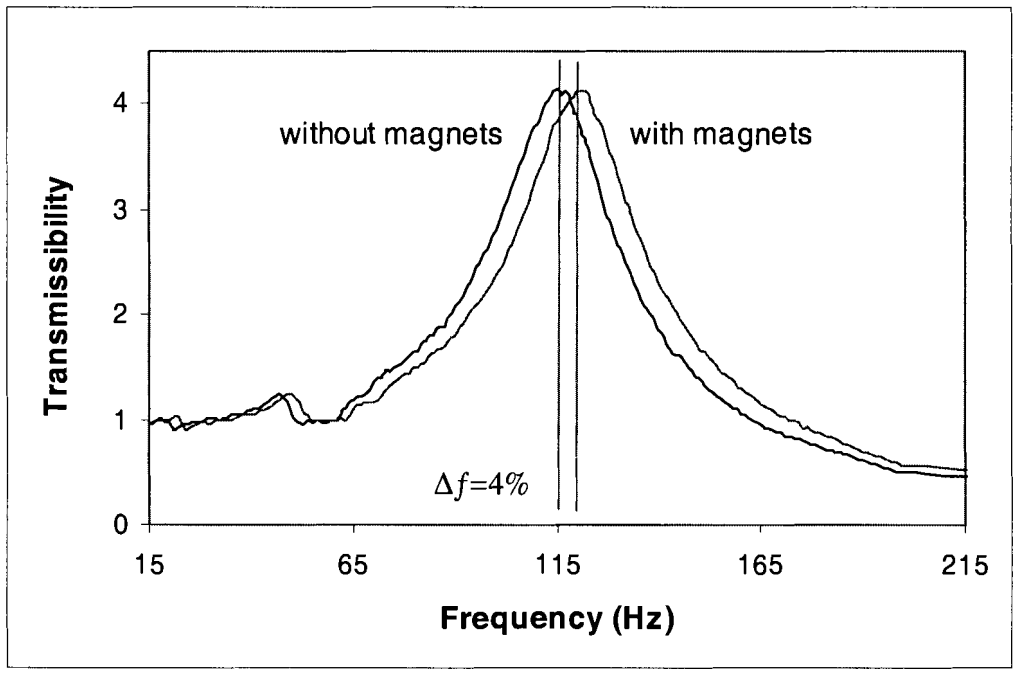

Figure 3.8: nMRE Response with a Mass of 375g

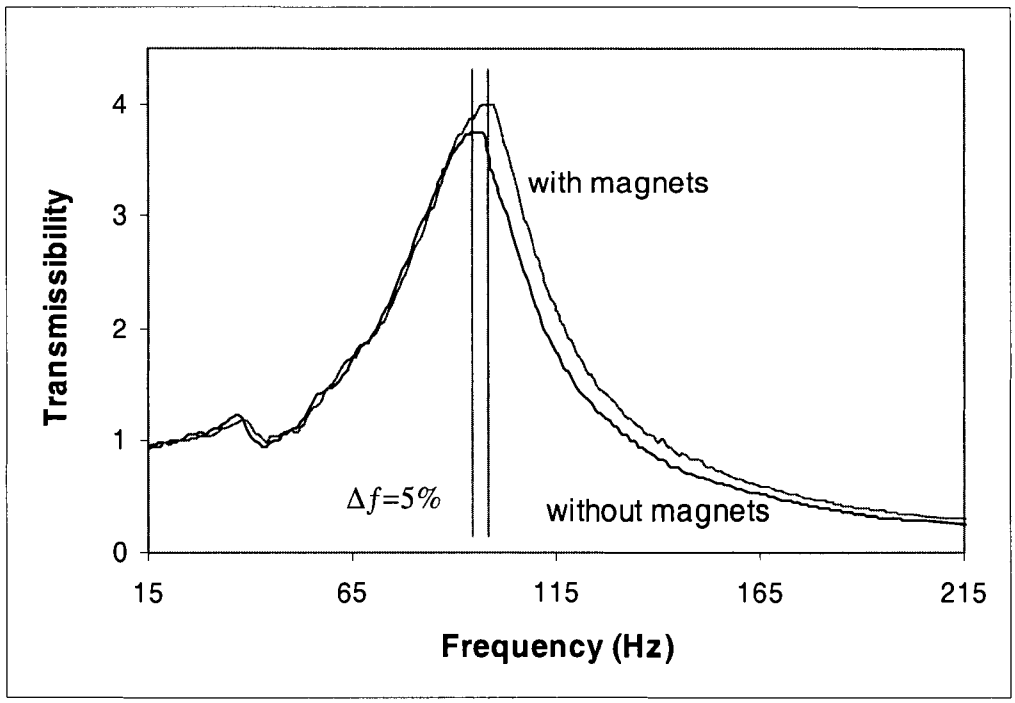

Figure 3.9: nMRE Response with a Mass of 575g

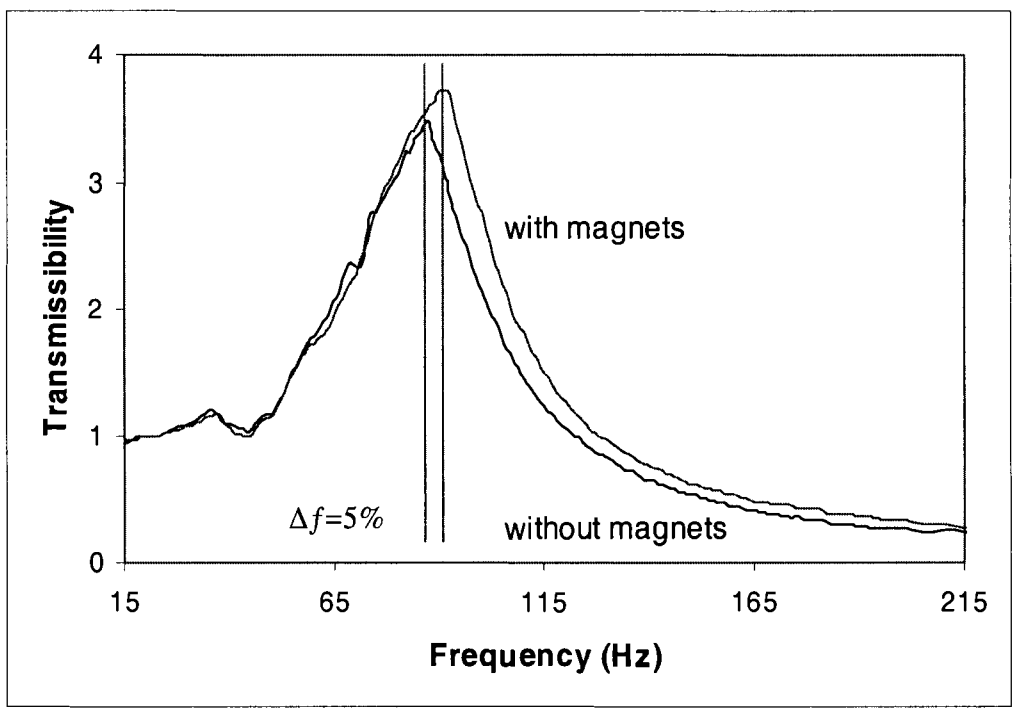

Figure 3.10: nMRE Response with a Mass of 675g

3.4.2 Experimental Results for the mMRE

The frequency response for the MRE cured within a magnetic field is shown in Figure 3.11, Figure 3.12, and Figure 3.13 for masses of 375g, 575, and 675g, respectively. Each graph contains a plot of transmissibility versus frequency for the MRE with and without a magnetic field. The fractional change in resonant frequency is labeled on each graph.

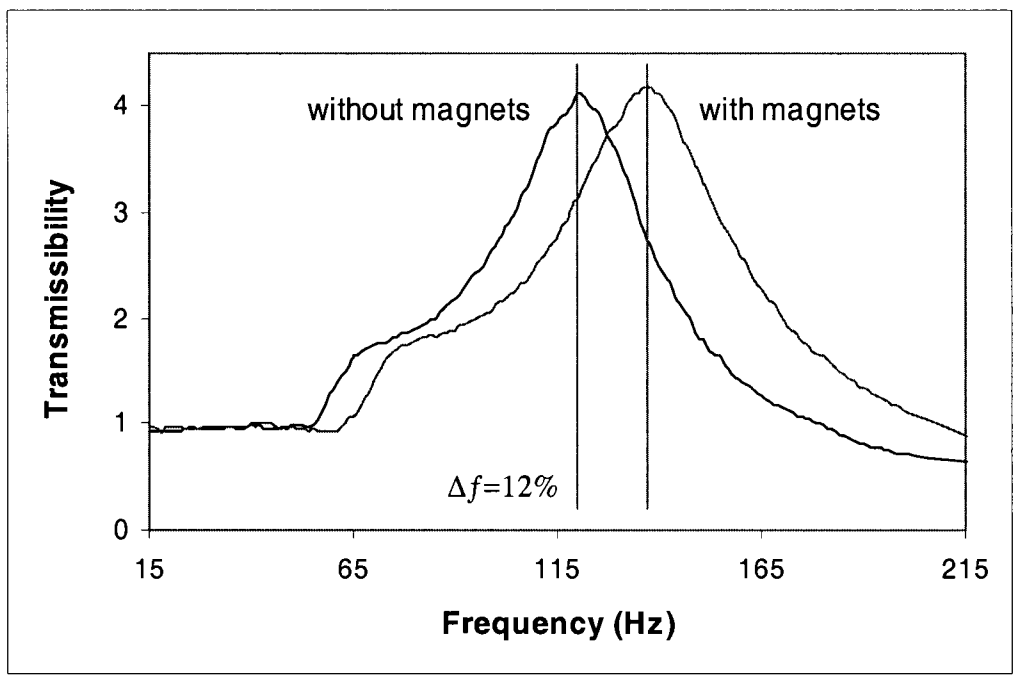

Figure 3.11: mMRE Response with a Mass of 375g

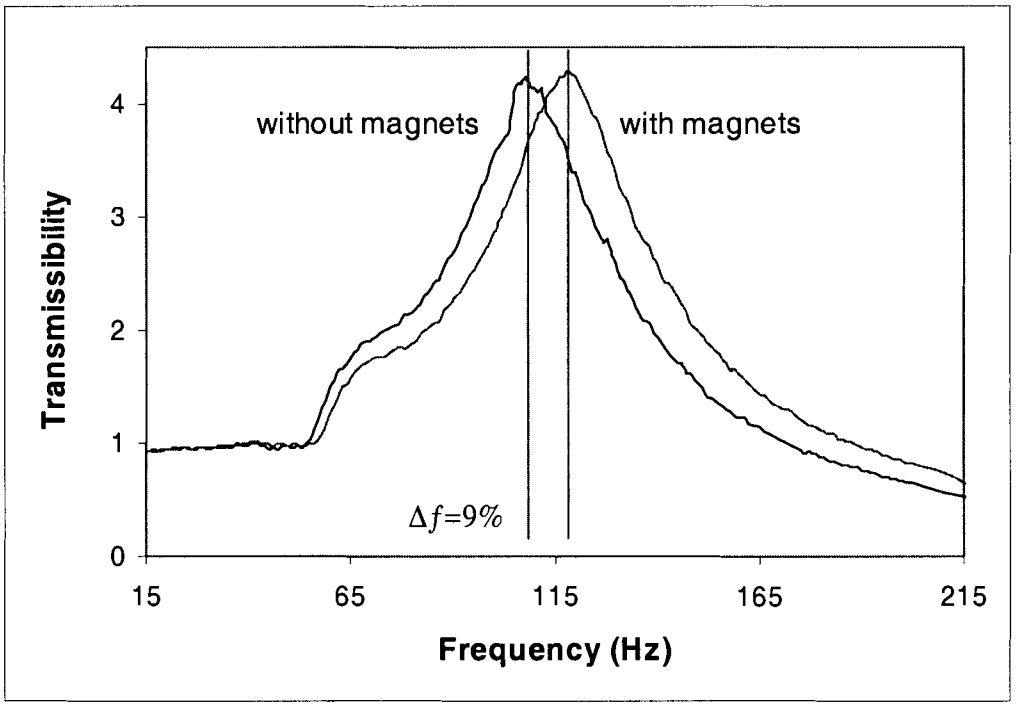

Figure 3.12: mMRE Response with a Mass of 575g

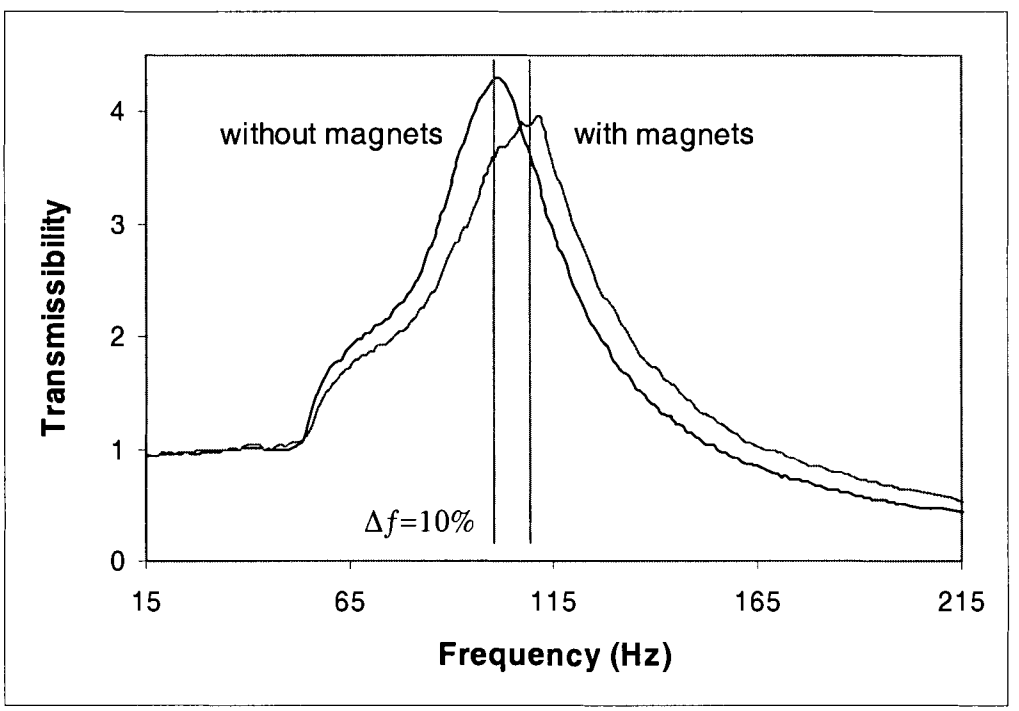

Figure 3.13: mMRE Response with a Mass of 675g

3.4.3 Discussion

Table 3.1 summarizes the resonant frequencies when a magnetic field is applied to the nMRE and mMRE. The table also shows the calculated percent change in the frequencies. Each value in the table has an error rating determined from our experimental procedure.

Table 3.1: Fractional Change in Resonant Frequency

	nMRE			mMRE		
mass (g)	f_0 (Hz)	f_1 (Hz)	$\frac{\Delta f}{f_0}$ (%)	f_0 (Hz)	f_1 (Hz)	$\frac{\Delta f}{f_0}$ (%)
375	117±1	122±1	4±2	121±1	136±1	12±2
575	95±1	100±1	5±2	108±1	118±1	9±2
675	87±1	91±1	5±2	101±1	111±1	10±2

When the MRE is not cured in a magnetic field, its resonant frequency is lower than the equivalent MRE cured in a magnetic field. Additionally, the change in resonant frequency is greater for the MRE cured in a magnetic field. For the nMRE, the average percent change of the natural frequency is 5% with a worst-case value of 3%. The average percentage change for the mMRE is 10% with a worst-case value of 8%.

Although the resonant frequency of the MRE changed when subjected to a magnetic field, we are unable to determine the change in amplitude around the resonant point. However, in most test cases, the transmissibility of the MRE at resonance was greater when a magnetic field was present. In two cases, nMRE with a 375g mass (see Figure 3.8) and for the mMRE with a 675g mass (see Figure 3.13), the amplitude at

resonance was greater without a magnetic field. We attribute this discrepancy to the test apparatus. We noticed that at the resonance point, the values obtained for the acceleration could vary. Experimentally, the resonance point was always within plus or minus 1 hertz. However, the amplitude would change by 5 to 10Vp-p.

For an MRE experiencing a shear force Jolly et al. [47], states that fractional change in modulus, $\Delta G/G_0$, is related to the fractional change in natural frequency, $\Delta\omega/\omega_0$, using

$$\frac{\Delta\omega}{\omega_0} = \sqrt{1+\frac{\Delta G}{G_0}} - 1. \qquad \text{Equation 3.4}$$

Solving for the fractional change in modulus yields

$$\frac{\Delta G}{G_0} = \left(\frac{\Delta\omega}{\omega_0}+1\right)^2 - 1. \qquad \text{Equation 3.5}$$

Assuming that the equation for the shear modulus can be applied to the elastic modulus when the stress is applied uniaxial to the material, we obtain the values for the fractional change in modulus shown in Table 3.2.

Table 3.2: Fractional Changes in Resonant Frequency and Modulus

	nMRE		mMRE	
mass (g)	$\frac{\Delta f}{f_0}$ (%)	$\frac{\Delta G}{G_0}$ (%)	$\frac{\Delta f}{f_0}$ (%)	$\frac{\Delta G}{G_0}$ (%)
375	4±2	9±4	12±2	26±4
575	5±2	11±5	9±2	19±4
675	5±2	10±5	10±2	21±5

The nMRE has an average change in modulus of 10% with an average worst-case value of 5% when the error margin is taken into account. Whereas, the mMRE has an average change in modulus of 22% with an average worst-case value of 18% when the error margin is taken into account. These results show that aligning the iron beads while the elastomer cures allows the applied magnetic field to have a greater effect on the change in modulus.

To verify the results obtained for the change in shear modulus, we assume that the system can be represented by a second order system at the resonant frequency. For a second order system shown in Figure 3.14, the governing mathematical equation is

$$M\ddot{x}_1 + k(x_1 - x_2) + C(\dot{x}_1 - \dot{x}_2) = 0. \qquad \text{Equation 3.6}$$

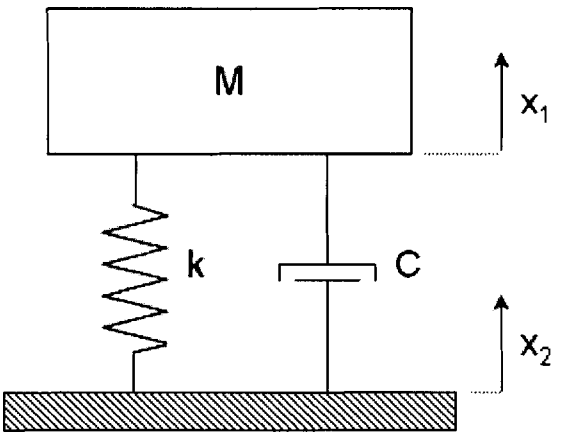

Figure 3.14: Second Order System

The transfer function for this system is

$$\frac{x_1(s)}{x_2(s)} = \frac{Cs + k}{ms^2 + Cs + k}. \qquad \text{Equation 3.7}$$

To solve for the resonant frequency, we substitute s=jω (where j represents an imaginary number) into Equation 3.7, solve for the magnitude (the real component of the complex number), and differentiate the equation with respect to the natural frequency. For a system with damping, the resonant frequency, ω_r, is

$$\omega_r = \sqrt{\frac{k}{m} - \frac{C^2}{2m^2}}. \qquad \text{Equation 3.8}$$

For each case, the only value that changes is the mass of the system, which causes a change in the resonant frequency. Let m_1 and m_2 be the mass used for two trials and ω_{r1} and ω_{r2} be the resonant frequency that results for each case, respectively. Solving Equation 3.8 for k for trial 1 gives

$$k = \frac{2m_1^2\omega_{r1}^2 + C^2}{2m_1}, \qquad \text{Equation 3.9}$$

and solving Equation 3.8 for C for trial 2 gives

$$C = \pm\sqrt{2m_2k - 2m_2{}^2\omega_{r2}{}^2}\,. \qquad \text{Equation 3.10}$$

Note that a negative value for the damping coefficient of a passive element has no physical meaning, therefore, Equation 3.10 can only have positive values. Substituting Equation 3.10 into Equation 3.9 and solving for k gives

$$k = \frac{m_1{}^2\omega_1{}^2 - m_2{}^2\omega_2{}^2}{m_1 - m_2}. \qquad \text{Equation 3.11}$$

Using Equation 3.10 and Equation 3.11, we calculated the damping and spring coefficients using the experimental values. We calculated the coefficients for three cases: a mass of 375g and 575g, a mass of 575g and 675g, and a mass of 375g and 675g. For each of these cases, we calculated k and C for each of the resonant frequency ranges determined via our experiments. The average values for the coefficients are summarized in Table 3.3 for the resonant frequency, f.

Table 3.3: Calculated Spring and Damping Coefficients

	MRE not cured in a magnetic field		**MRE cured in a magnetic field**	
	k (N/m)	C (N/(m/sec))	k (N/m)	C (N/(m/sec))
No field	5,452	16	8,579	46
With field	6,026	19	10,053	48
Δ	574	3	1,474	2

The spring coefficient, k, is directly related to the modulus of elasticity. The units for the modulus of elasticity are N/m^2 and the units for the spring coefficient are N/m. If the

dimensions of the MRE are not changing between our tests, then we can directly compare the change in k to a change in the Modulus of Elasticity. Therefore, using the values for k obtained in our analysis, we can determine the fractional change in the Modulus of elasticity, which are 10% for the nMRE and 17% for the mMRE. These results are consistent with the previous results, that directly use Equation 3.5. However, when the mass of the system decreases, ignoring the damping coefficient will lead to inaccurate predictions of the resonant frequency. This inaccuracy is easily shown by substituting our calculated values for the spring and damping coefficients into Equation 3.8. The graph for this equation is plotted in Figure 3.15.

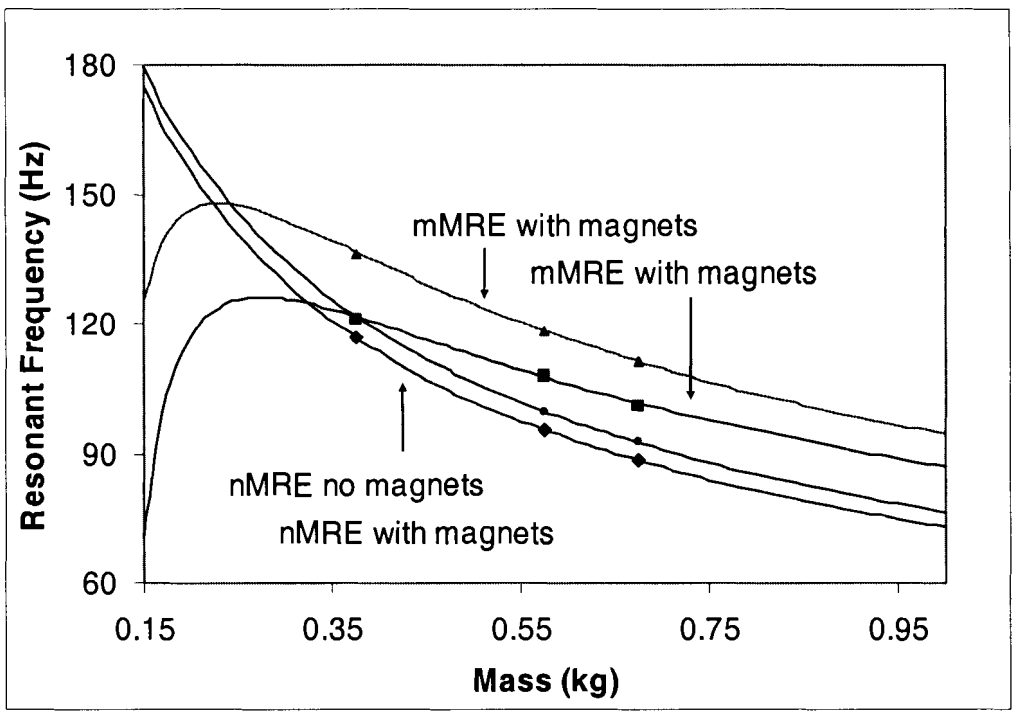

Figure 3.15: Resonant Frequency versus Mass

In the graph, the points plotted are the values we measured for the resonant frequency. As shown, these values are on the calculated curves we created assuming that the system can be modeled as a second order system. This graph allows us to determine the resonant

frequency associated with a mass. Notice that as the mass becomes smaller, the resonant frequency decreases. If the damping coefficient was neglected then we would not see this effect.

3.4.4 Magnets Placed Traverse to Elastomer

We conducted additional experiments with the nMRE where, instead of placing the magnets on top of the MRE as in the previous experiments, we placed the magnets on the side of the MRE as shown in Figure 3.16.

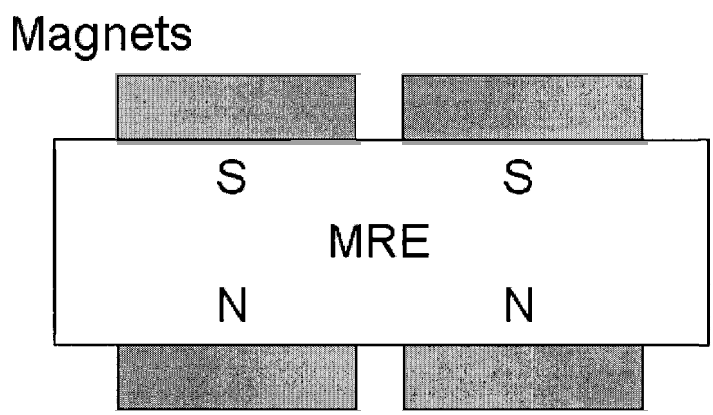

Figure 3.16: Top View of the nMRE with Magnets on the Side

The pole of the magnet closest to the MRE is labeled in the figure. The field is now perpendicular to the direction of acceleration. The magnets that are on the same side of the MRE will repel each other, while the magnets across from each other will attract. This configuration ensures uniform field lines throughout the elastomer. The magnetic field lines are traverse to the direction of acceleration.

We also conducted other experiments where we altered the position of the magnets so that the magnets on the same side of the MRE were attracted to each other as

well as being attracted to the magnets on the other side of the elastomers. This new configuration is illustrated in Figure 3.17.

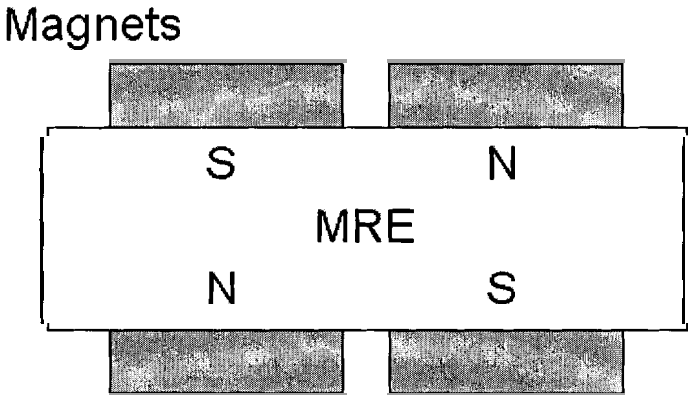

Figure 3.17: Top View of nMRE with Magnets to the Side

We conducted these experiments with a mass of 875g. The results with no magnets, and magnets for configuration 1 (C1) and configuration 2 (C2) are plotted in Figure 3.18.

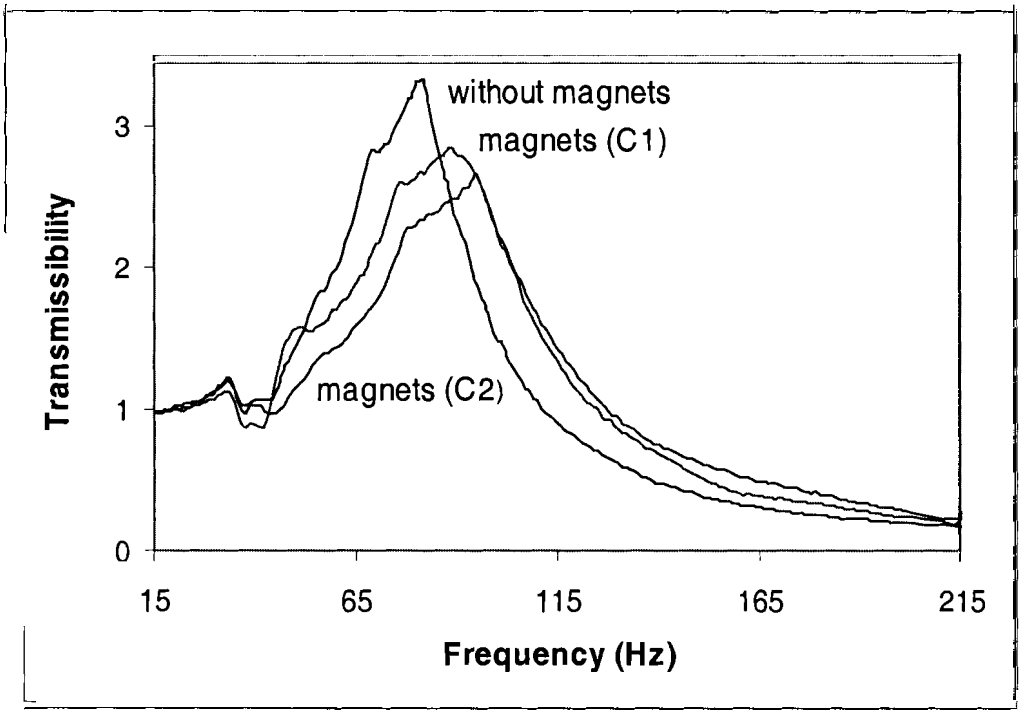

Figure 3.18: nMRE with Alternative Magnet Configurations

The graph shows that the properties of the MRE change when the magnetic field is perpendicular to the direction of motion. Similar to the other experiments, the natural frequency moves to a higher frequency. Note how configuration 1 and 2 give similar results after 100Hz. Before this frequency, however, configuration 1 has a greater transmissibility.

We are unsure why this change occurs with the different magnet configurations. Intuitively, we expected configuration 1 to yield a larger change in the resonance frequency because the field was uniform. We tried reproducing this experiment with the mMRE but we did not obtain similar results. The beads may need a random configuration to produce the measured effects.

3.5 Contributions and Conclusions

3.5.1 Contributions

The results from thesis have shown the following:

- A magnetorheological elastomer fabricated from silicone and iron beads (45-70μm in diameter) when subject to a magnetic field changes its spring and damping coefficients. Because these parameters can be altered, the resonant frequency of the system can be controlled.
- A magnetorheological elastomer with beads aligned while the matrix material cures has a higher spring and damping coefficient than a magnetorheological elastomer that has a uniform bead distribution.

- The change in damping coefficient does not change significantly for either type of elastomer when a magnetic field is introduced. The spring coefficient for the elastomer with aligned particles has a greater change in spring constant.
- When designing a system with a high damping coefficient and a low mass, the damping coefficient must be used to determine the resonant frequency (see Figure 3.15 and Equation 3.8).
- Curing the elastomer so that the beads do not settle requires that the silicone matrix start curing before the iron beads are mixed into the elastomer.

3.5.2 Conclusion

We successfully created two magnetorheological elastomers (MRE) using silicone and 30 percent iron beads by volume. The first MRE we created had the beads evenly distributed throughout the silicone matrix while the second MRE was cured in a magnetic field so that the iron beads formed chain-like structures. The resonant frequency of both MREs changed when a magnetic field was applied. Using three masses for our system we calculated the spring and damping coefficients assuming that the system at resonance is modeled by a second order system. Our measured data agrees with our calculated curves.

We also determined that magnets perpendicular to the direction of acceleration have an affect on the MRE. When we measured the transmissibility of the MRE with magnets placed traverse to the direction of acceleration, we obtained different results than expected.

The first stage in our three phase research for controlling structure-borne noise is now complete. This thesis has outlined integral information needed for the successful completion of the following two research stages. In order to develop a final product, future work as outlined in section 3.6 needs to be accomplished.

3.6 Future Work

Future experiments will incorporate an electromagnet so that the magnet field intensity can be varied. This addition of a variable field sources will allow a third axis to be added to Figure 3.15 involving field strength. In order for the electromagnet to be utilized a step-up DC-DC converter to be used as a power amplifier must be designed.

Additionally, the test setup needs to incorporate a sensor such as a linear variable differential transformer (LVDT) in order to measure the change in height of the MRE. This measurement will allow the strain to be measured so that direct comparisons of the modulus of elasticity can be made for the case of no magnetic field versus a magnetic field.

REFERENCE LIST

[1] R. A. Shoureshi, R. Gasser, J. Vance, "Automotive applications of a hybrid active noise and vibration control", IEEE *Control Systems Magazine*, vol. 16, no. 6, pp. 72-28, December 1996.

[2] Auto21, "Research, Intelligent Systems and Sensors", 2005 "http://www.auto21.ca/intelligentsystems_3interior_e.html"

[3] B. Riley, M. Bodie, "An adaptive strategy for vehicle vibration and noise cancellation," *Proceeding of the IEEE Aerospace and Electronics Conference*, vol. 2, pp. 836-843, May 1996.

[4] D. Hrovat, "Survey of advanced suspension developments and related optical applications," *Automaticia*, Vol. 33, no. 10, pp. 1781-1817, October 1997.

[5] P. M. Fishbaine, S. Gasiorowicz, and S. T. Thornton, *Physics for Scientists and Engineers*, New Jersey: Prentice Hall, 1996.

[6] A. B. Wright and A Karthikeyan, "Experimental characterization of the near field zones of silence in an active sound cancellation scheme," *IEEE/ASME International Conference on Advanced Intelligent Mechanics,* pp. 842-847, September 1999.

[7] S. H. Yu and J. S. Hu, "Controller design for active noise cancellation headphones using experimental raw data," *IEEE/ASME Transactions on Mechatronics*, vol. 6, no. 4, pp. 483-490, December 2001.

[8] B. Rafaely and S. J. Elliott, "H_2/H_∞Active Control of Sound in a Headrest: Design and Implementation," *IEEE Transactions on Control Systems Technology*, vol. 7, no. 1, pp. 79-84, January 1999.

[9] S. P. Nagarkatti, "Keeping the noise down in confined spaces," *IEEE Potentials*, pp. 29-31, August/September 2001.

[10] H. Sano, T. Inoue, A. Takahashi, K. Terrai, and Y. Nakamura, "Active Control System for Low-Frequency Road Noise Combined With an Audio System," *IEEE Transactions on Speech and Audio Processing*, vol. 9, no. 7, pp. 755-763, October 2001.

[11] S. J. Elliot, "Down with Noise: "Practical control systems for combating audible noise show up in aerospace, general aviation, and military roles," *IEEE Spectrum*, pp. 54-59, June 1999.

[12] S.J Elliot and P.A. Nelson, "The Active Control of Sound," *Electronics & Communication Engineering Journal*, vol. 2, no. 4, pp. 127-136, August 1990.

[13] R. Cabell, D. Palumbo, and J. Vipperman, "A principal component feedforward algorithm for active noise control: flight test results," *IEEE Transactions on Control System Technology*, vol. 9, no. 1, pp. 76-83, January 2001.

[14] V. V. Varadan, Z. Wu, S-Y. Hong, and V. K. Varadan, "Active Control of Sound Radiation from a Vibrating Structure," *IEEE Ultrasonic Symposium*, vol. 2, pp. 991-994, 1991.

[15] H.S. Tan, T. Bradshaw, "Model Identification of an Automotive Hydraulic Active Suspension System", *Proceedings of the American Control Conference*, vol. 5, pt. 5 pp. 2920-2924, June 1997.

[16] J. S. Lin, I. Kanellakopoulos, "Nonlinear Design of Active Suspensions", *34 IEEE Conference on Decision and Control*, vol. 4, pt. 4, pp 3567-3569, December 11-13, 1995.

[17] K. Ogata, *Modern Control Engineering*, Third Edition, New Jersey: Prentice Hall, 1997.

[18] R. A. Williams, "Control of a Low Frequency Active Suspension", *Control '94*, IEE 1994, vol.1, pt.1 pp. 338-343, March 21-24, 1994.

[19] R. S. Sharp, "Variable geometry active suspension for cars", *Computing & Control Engineering Journal*, vol. 9, no. 5, pp. 217-222, October 1998.

[20] M. Appleyard, P.E. Wellstead, "Active suspensions: some background", *IEE Proc.-Control Theory Applied*, vol. 142, no. 2, pp 123-128, March 1995

[21] A.W. Burton, "Active vibration control in automotive chassis systems", *Computing & Control Engineering Journal*, vol. 4, no. 5, pp. 225-232, October 1993.

[22] J. Li, W. A. Gruver, "An electrorheological fluid damper for vibration control", *Proceedings of the 1998 IEEE International Conference on Robotics & Automation*, vol. 3, pt. 3, pp. 2476-2481, May 1998.

[23] H. R. O'Neill, G. D. Wale, "Semi-active suspension improves rail vehicle ride", *Computing & Control Engineering Journal*, vol. 5, no. 4, pp. 183-188, August 1994.

[24] A. Titli, S. Roukieh, E. Dayre, "Three control approaches for the design of car semi-active suspension (optimal control, variable structure control, fuzzy control)", *Proceedings of the 32nd Conference on Decision and Control*, vol. 3, pt. 3, pp. 2962-2963, December 1993.

[25] S. Sadok, K. Cherif, M. Thomas, "On the design and testing of a smart car damper on electro-rheological technology", *Smart Materials and Structures*, vol. 12, pp. 873-880, 2003.

[26] S. Rakheja, S. Sankar, "Vibration and shock isolation of a semi-active 'on-off' damper", *Transactions of the ASME Journal of Vibration, Acoustics, Stress, and Reliability Design*, vol. 107, iss. 4, pp. 398-403, 1985.

[27] Y. Shen, M. F. Golnaraghi, G. R. Heppler, "Semi-active suspension control with a magnetorheological damper", Smart *Materials and Structures, 7th Cansmart Workshop*, pp. 143-152, October 2004.

[28] H. Ware, "Early Falcon Car Club", 2004, *"http://www.stormloader.com/falconccwa/front1hint.htm"*

[29] H. Douville, "An approach using active structural acoustic control for the reduction of structure-borne road noise", Master Thesis Faculty of Engineering, Mechanical Engineering Department, Sherbrooke University, Quebec Canada, 2003.

[30] "MR Fluids and Devices", 2004, *"http://cee.uiuc.edu/sstl/gyang2/Ch2.pdf"*.

[31] M. R. Jolly, J. W. Bender, J. D. Carlson, "Properties and applications of commercial magnetorheological fluids," *Proceedings of the SPIE – The International Society of Optical Engineering*, vol. 3327, pp 262-275, 1998.

[32] G. M. Kamath, N. M . Wereley, "A nonlinear viscoelastic-plastic model for electrorheological fluids," IOP Publishing Ltd., 1997 *http://pbl.cc.gatech.edu/bmed8101/uploads/432/KamathSMSVol6No3.pdf*

[33] J. D. Carlson, "Magnetorheological fluids — ready for real-time motion control," Lord Corporation, Materials Division, Cary North Carolina, USA, 2005 *http://cee.uiuc.edu/sstl/Beijing_Symposium/p-38/III-3.Carlson.pdf*

[34] N. Takesue, A. Asaoka, J. Lin, M. Sakaguchi, G. Zhang, J. Furusho, "Development and experiments of actuators using MR fluid", *IEEE International Conference on Industrial Electronics, Controls and Instrumentation, 21st Century Technologies and Industrial Opportunities*, vol. 3, pt. 3, pp. 1838-1843, *2000.*

[35] T. Simon, F. Reitich, "Modeling and computation of the overall magnetic properties of magnetorheological fluids," *Proceedings of the 36th Conference on Decision and Control*, vol. 4. pt. 4, pp 3721-3726, December 1997.

[36] J. U. Cho, Y. Choi, N.M. Wereley, "Constitutive models of electrorheological and magnetorheological fluids using viscometers," *Proceedings of SPIE* Vol. 5052, pp. 66-82, July 2003.

[37] G. T. A Kovacs, *Micromachined Trasnducers: Sourcebook*, Toronto: WCB, McGraw-Hill: 1998.

[38] J. M. Ginder, M. E. Nichols, L. D. Elie, S. M. Clark, "Controllable-stiffness components based on Magnetorheological elastomers," *Smart Structures and Integrated Systems,* vol. 3985, pp. 418-425, 2000.

[39] Y. Shen, M. F. Golnaraghi, G. R. Heppler "Experimental research and modelling of magnetorheological elastomer," *Journal of Intelligent Material Systems and Structures*, vol. 15, no. 1, pp. 27-35, January 2004.

[40] G. Y. Zhou, "Shear properties of a magnetorheological elastomer," *Smart Material Structures*, vol. 12. pp. 139-146, 2003.

[41] A. J. Margida, K. D. Weiss, J. D. Carlson, "Magnetorheological materials based on iron alloy particles," *Proceedings of the 5th International Conference on Electro-rheological fluids, Magnetorheological Suspensions and Associated Technology*, pp. 544-550, 1996.

[42] M. Lockander, B. Stenberg, "Performance of isotropic magnetorheological rubber materials", *Polymer Testing*, vol. 22, no. 3, pp 245-251, 2003.

[43] A. Albanese, K. A. Cunefare, "Smart fabric adaptive stiffness for active vibration absorbers," *Smart Structures and Materials*, SPIE vol. 5383, pp. 490-497, 2004.

[44] S. Toru, F. Shigeru, H. Miharu, O. Akane, K. Norio, U. Osami, "Material having magnetic response", Japanese Patent, JP5025316, Applicant: Toyota Central Res & Dev Lab Inc., February '2, 1993.

[45] L. Borcea, O. Bruno, "On the magneto-elastic properties of elastomer-ferromagnet composites," *Journal of the Mechanics and Physics of Solids*, vol. 49, no. 12, pp 2877-2919, December 2001.

[46] G. Y. Zhou, Z. Y Jiang, "Deforamtion in magnetorheological elastomer and elastomer-ferromagnet composite driven by a magnetic field, *Institute of Physics Publishing, Smart Materials and Structures*, vol. 13, pp. 309-316, 2004.

[47] M. R. Jolly, J. D. Carlson, B. C. Munoz, T. A. Bullions, "The magnetoviscoelastic response of elastomer composites consisting of ferrous particles embedded in a polymer matrix," *Journal of Intelligent Material Systems and Structures*, vol. 7, no. 6, pp. 613-622, November 1996.

APPENDICES

APPENDIX A:
MAGNTEORHEOLOGICAL BUSHING CONSTRUCTION PROCEDURE

The following steps were used to create the semi-active bushing using magnetorheological fluid.

We modified an Energy Suspension G.M. 4WD Front Spring Bushing (#2006). The package was bought at Lordco Auto Parts and is shown in Figure A- 1.

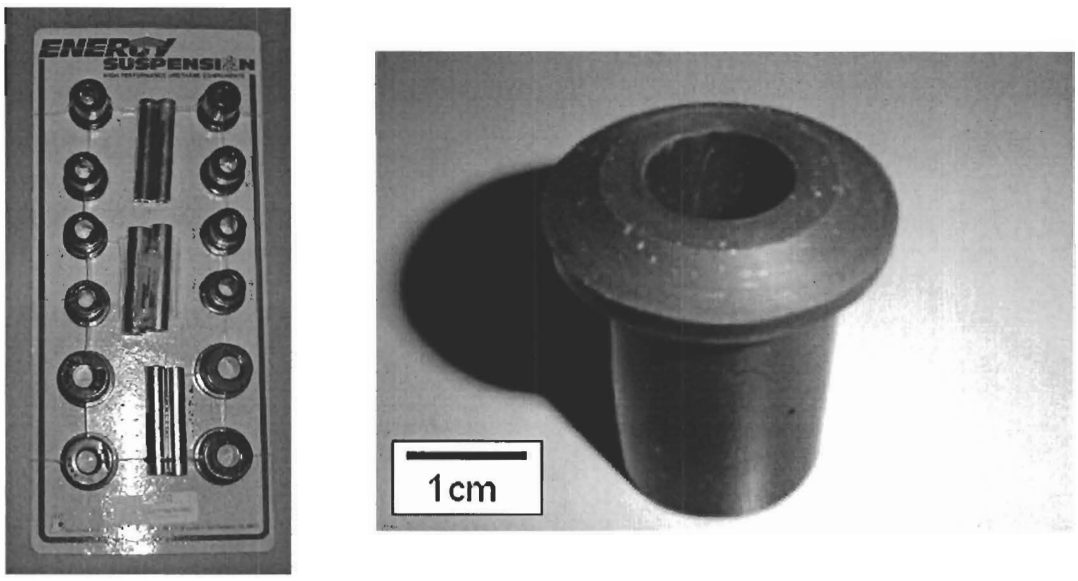

Figure A- 1: Bushings Used to Create the Semi-active Bushing

We placed a hard piece of rubber on the lathe and used a file to remove the material from the center. We used a milling machine to increase the inner diameter of the store bought bushing in order to accommodate the machined piece of rubber. Figure A- 2 shows the material on the lathe and the milling machine used.

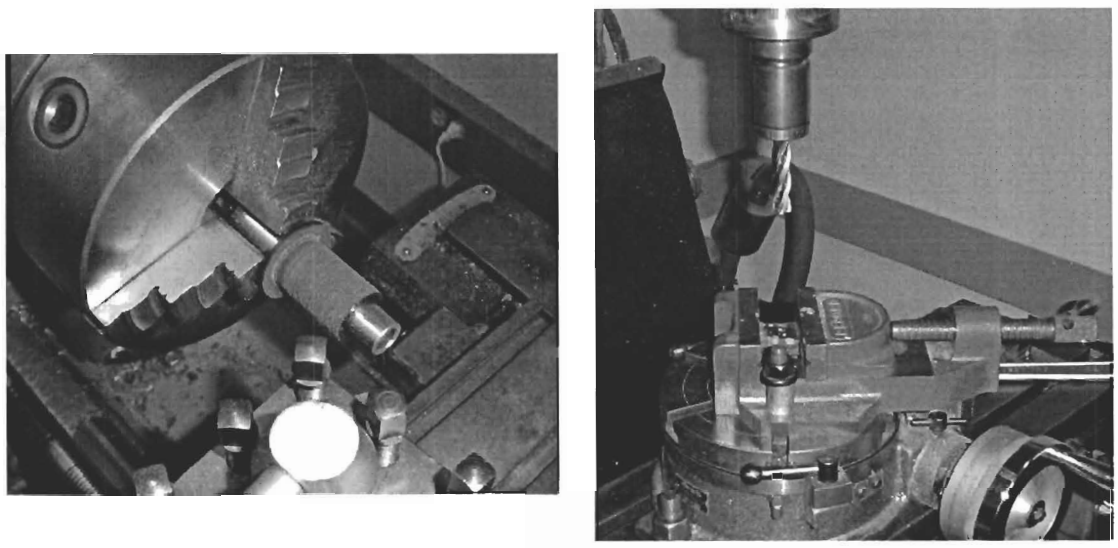

Figure A- 2: Machining of Parts

Once the rubber was machined, we drilled two holes in the side and placed hollow metal cylinders inside to keep the holes open. Figure A- 3 shows a side and front view of the machined piece of rubber.

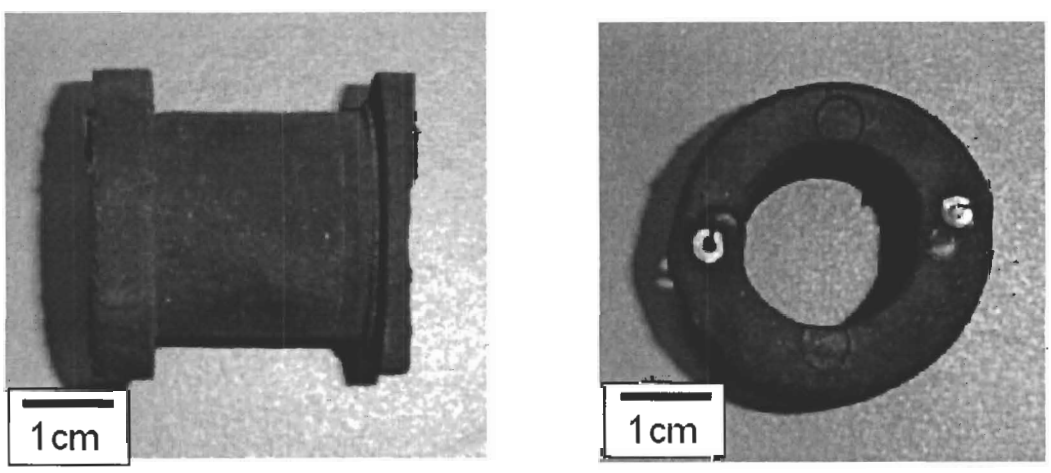

Figure A- 3: Machined Piece of Rubber

We affixed a piece of polymer to the end of the machined piece of rubber to cover the through holes. The polymer allows the MRF to flow out of the cavity. Figure A- 4

shows the rubber with the polymer attached before it has been cut to shape as well as the rubber in the housing with a piece of neoprene to provide a restoring force.

Figure A- 4: Polymer and Neoprene

The final stage for producing the semi-active bushing is to place an end cap over the neoprene to ensure all components stay in the housing. A picture of the end-cap and the top view of the completed bushing are illustrated Figure A- 5.

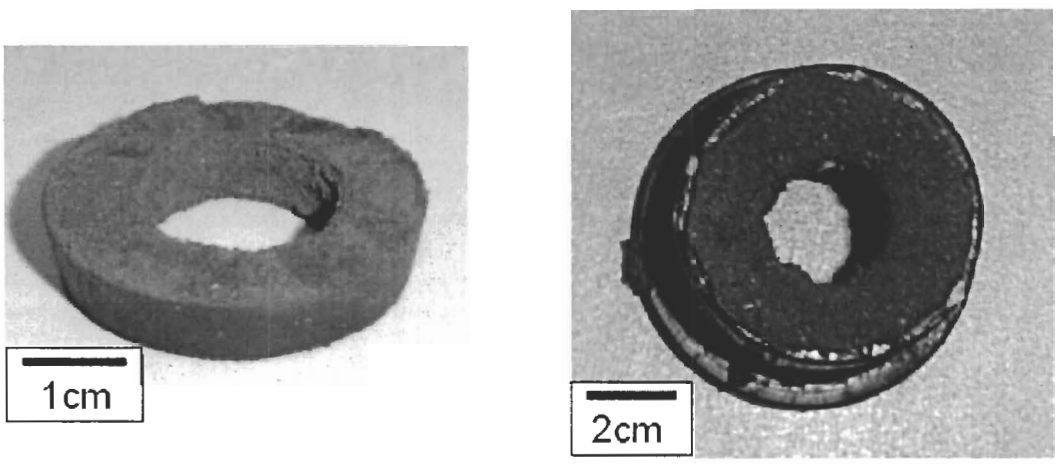

Figure A- 5: Endcap and Final Version of the Bushing

We modified the iron bar that came with the bushing to accommodate two metal connectors. A bushing with the metal rod inserted through it is shown in Figure A- 6 as well as the assembly used to add mass to the test set-up.

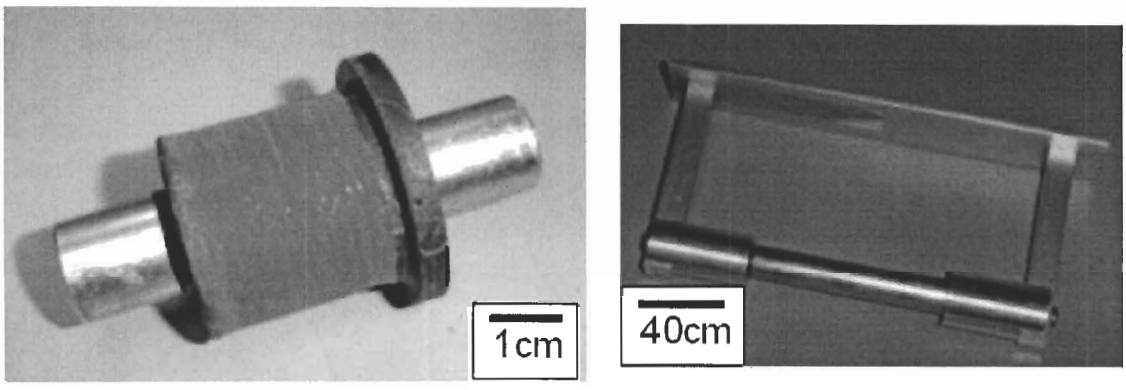

Figure A- 6: Bushing Rod and Mass Connector

The bushing is placed through the aluminum test housing as shown in Figure A- 7.

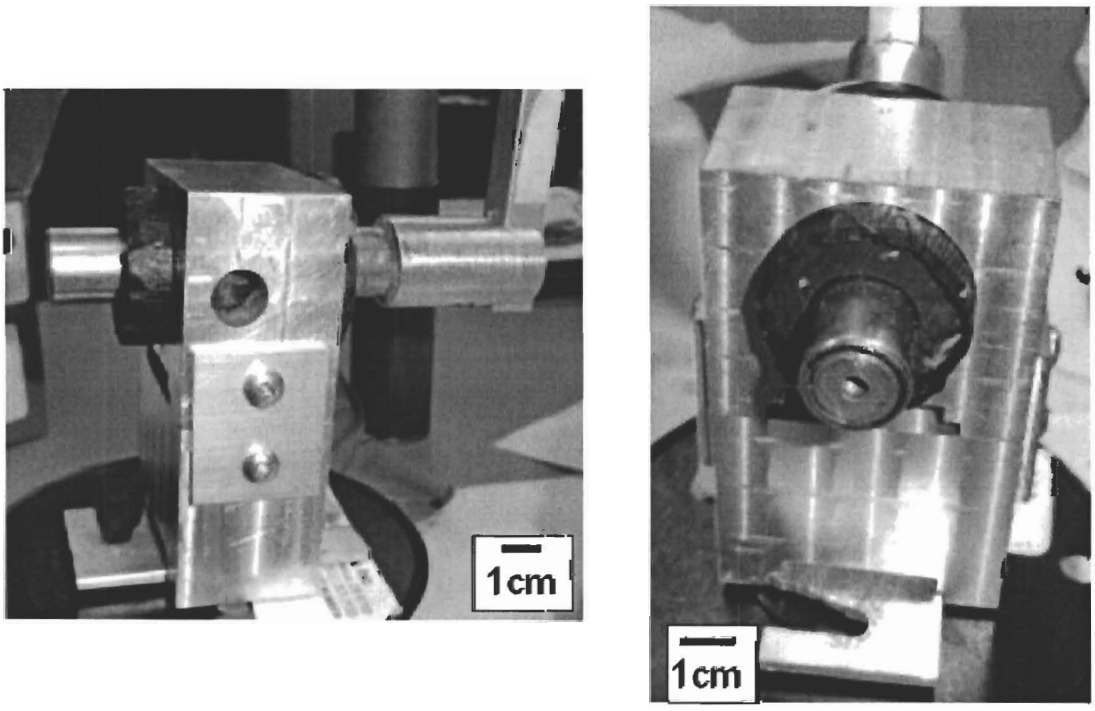

Figure A- 7: Test Rigging

Once the bushing is in place, the metal connector used to hold the mass is connected. The final test structure is shown in Figure A- 8.

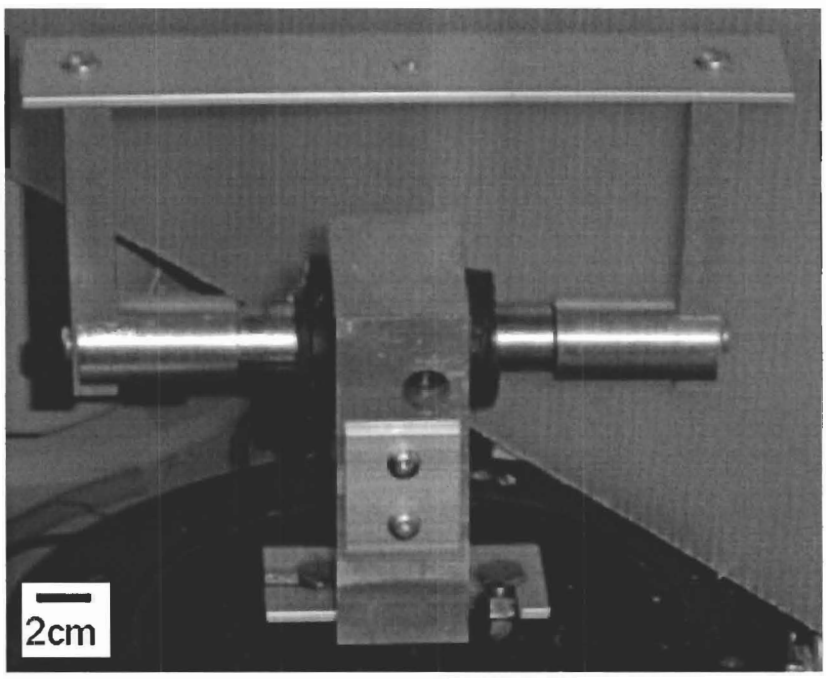

Figure A- 8: Final Test Rigging Configuration

The holes in the side of the aluminum housing is where we place the magnets into the system.

APPENDIX B:
DEMODULATION USING AN ATMEL MICROCONTROLLER

We used an Atmel AT90S8515 AVR microcontroller (see Figure B- 1) for the experiments involving the semi-active bushing using magnetorheological fluid. We needed the microcontroller in order to demodulate the signal coming from the Analog Devices ADXL210 accelerometers.

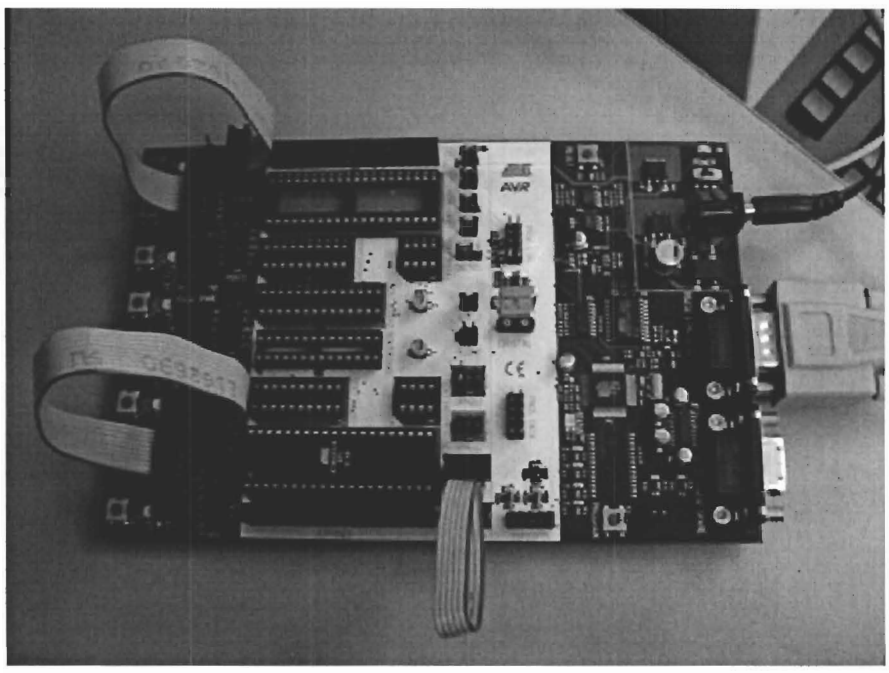

Figure B- 1: Atmel AT90S8515 AVR Microcontroller

Figure B- 2 shows the accelerometer mounted on the PCB we created. The schematic for the circuit is shown in Figure B- 3.

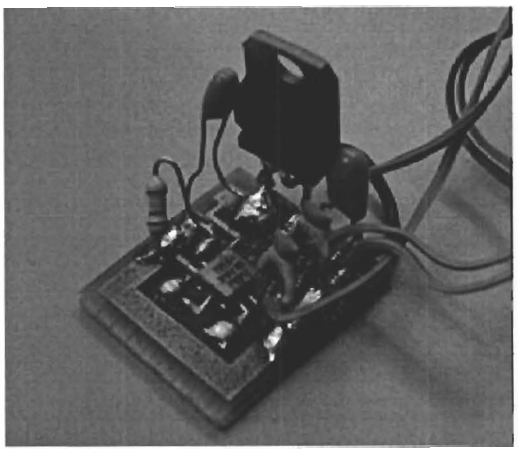

Figure B- 2: Accelerometer PCB

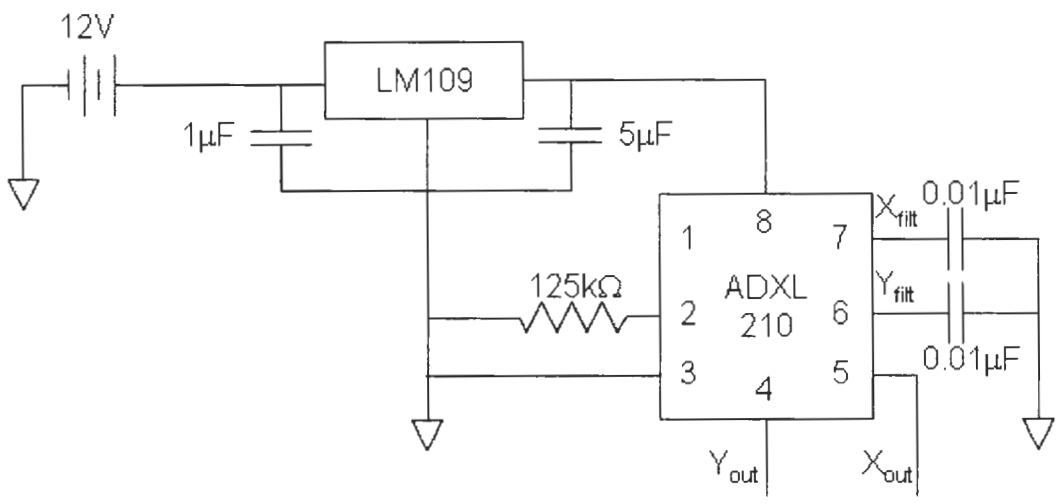

Figure B- 3: Circuit Schematic for the Accelerometers

The LM109 is a 5volt regulator. The output pins, X_{out} and Y_{out}, of the accelerometer produce a duty cycle modulated (DCM) signal as shown in Figure B- 4.

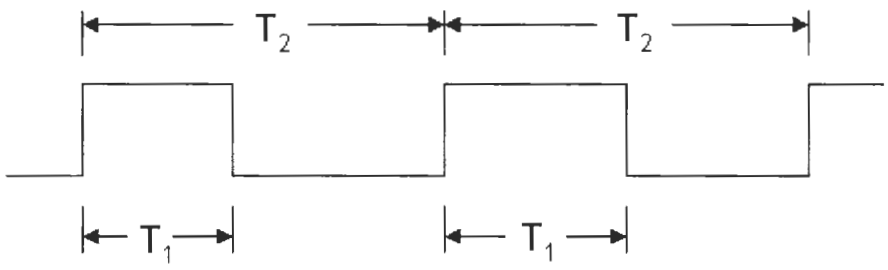

Figure B- 4: DCM Signal Generated by the Accelerometer

To calculate the acceleration, *A*, from the DCM signal, Equation 3.12 is used

$$A = \frac{\frac{T_1}{T_2} - 0.5}{0.04}, \qquad \text{Equation 3.12}$$

where T_1 and T_2 are as defined in Figure B- 4, and the 0.04 accounts for a 4% scale factor. The time for T_2 is set by the resistor R_{set} using the formula

$$T_2 = \frac{R_{set}}{125M}. \qquad \text{Equation 3.13}$$

For our circuit, R_{set} is equal 125Ω setting T_2 equal to 1ms.

APPENDIX C:
MAGNETORHEOLOGICAL ELASTOMER FABRICATION PROCEDURE

When we created the MRE we had to ensure that it could be attached to the shaker table assembly and the magnet holder (see appendix C for an explanation of the test setup). Our solution was to mold screws directly into the silicon elastomers. The screws, washers, and nut assembly is shown in Figure C- 1.

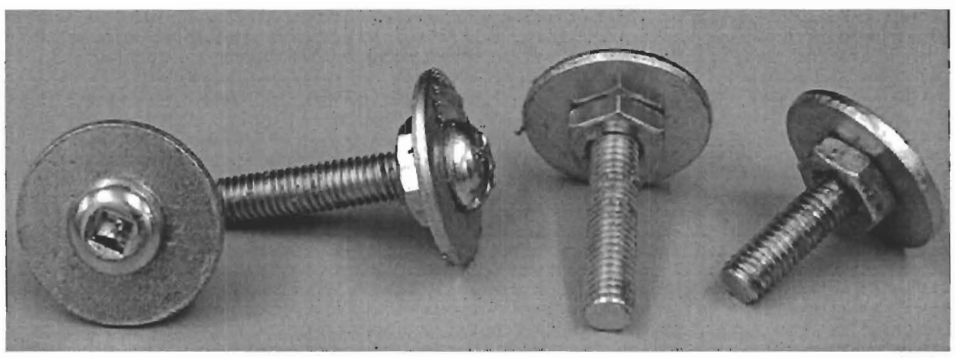

Figure C- 1: Screw Assembly Used for the MRE

We used a large washer to increase the area of contact between the screw head and the MRE. The nut is used as a spacer and allows the MRE to fully enclose the washer when curing. Figure C- 2 shows two of the screw assemblies attached to a piece of sheet metal used when curing the MRE. A second nut is used to keep the screws in place during the molding process. Note, the spacing provided by the first nut is clearly visible.

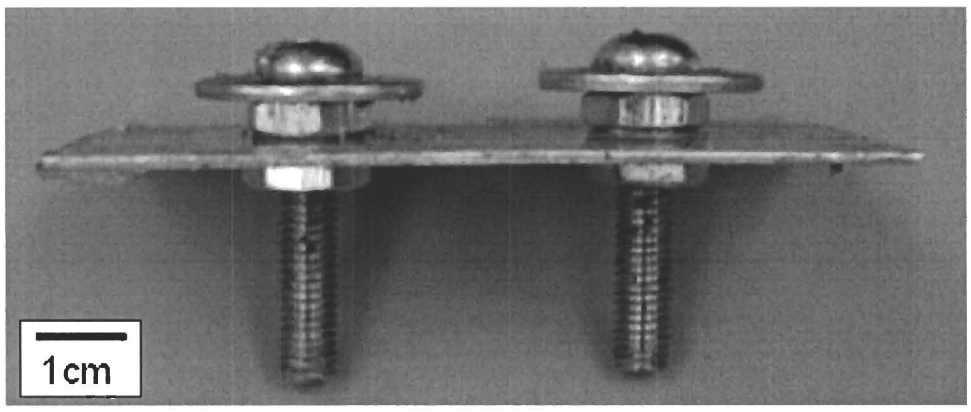

Figure C- 2: Screw Assemblies Mounted on Sheet Metal

To cure the MRE, we created a molding box using two of the assemblies shown in Figure C- 2, two smaller side plates, and a bottom plate. The mold assembly is illustrated in Figure C- 3.

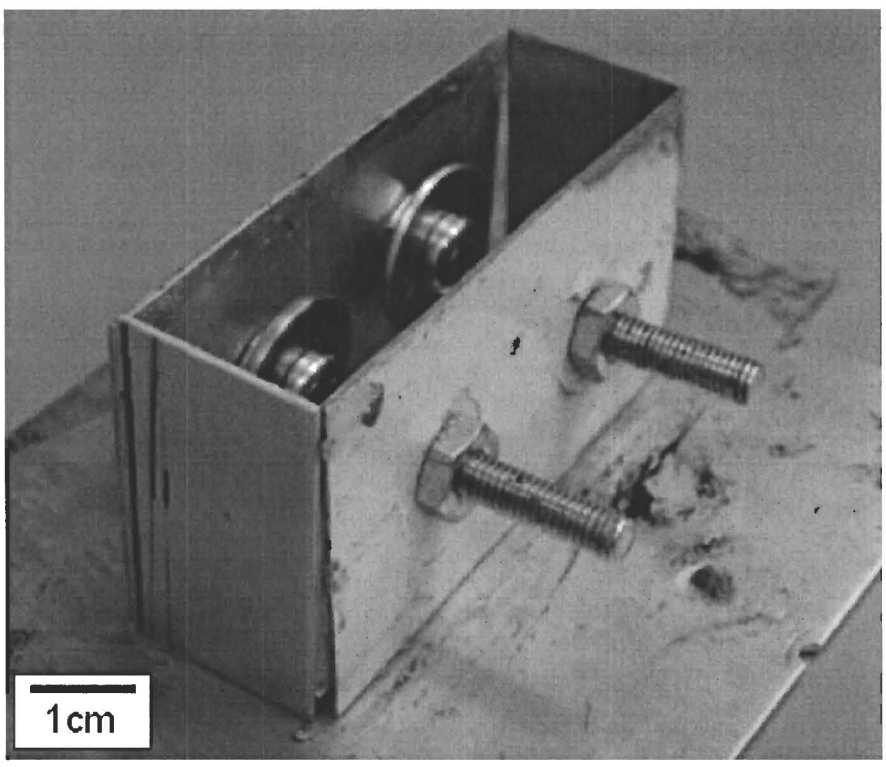

Figure C- 3: MRE Mold

Before the silicone and beads are cured in the assembly, plumber's putty is used to close any gaps in the metal plates.

We discovered through preliminary experiments that the iron beads settled in the silicone matrix. In order to create an MRE where the beads did not settle, we had to start the curing of the silicone before the beads were introduced into the mixture. As the silicone cures, its viscosity increases. The beads will not settle if the silicone is thick enough. To create the MRE, we used the following procedure:

1. Preheat an oven to 85°C.
2. Using Sylgard's Brand 184 silicone elastomer, measure 10 parts of the base to 1 part of the curing agent by weight. In our case, we used 43g to 4.3g.
3. Thoroughly stir the base and curing agent together.
4. Measure 20mL of Alfa Aesar's iron beads (mesh size of - 40+70 (45-70μm in diameter)).
5. Place the mold assembly, mixed silicone, and iron beads in the preheated oven.
6. Stir the silicone at 10 minutes for 30 seconds to help remove any air bubbles.
7. When the viscosity of the silicone is similar to thick syrup (approximately 20 minutes), stir in the iron beads slowly. If the beads are stirred in all at once, their weight will case them all to sink to the bottom of the container.
8. Stir the silicone bead mixture every 2 minutes until settling no longer occurs.
9. Approximately at the 26 minute mark, the silicone/bead mixture can be poured into the mold.
10. Place the mold into the oven and introduce a magnetic field if the beads need to form chains. For our experiments we used a magnetic field of 0.07T.

11. At 50 minutes, the silicone should be solid and the mold can be removed from the oven. Let the assembly cool to room temperature before removing the MRE.

The cured MRE while still in the mold assembly is shown in Figure C- 4.

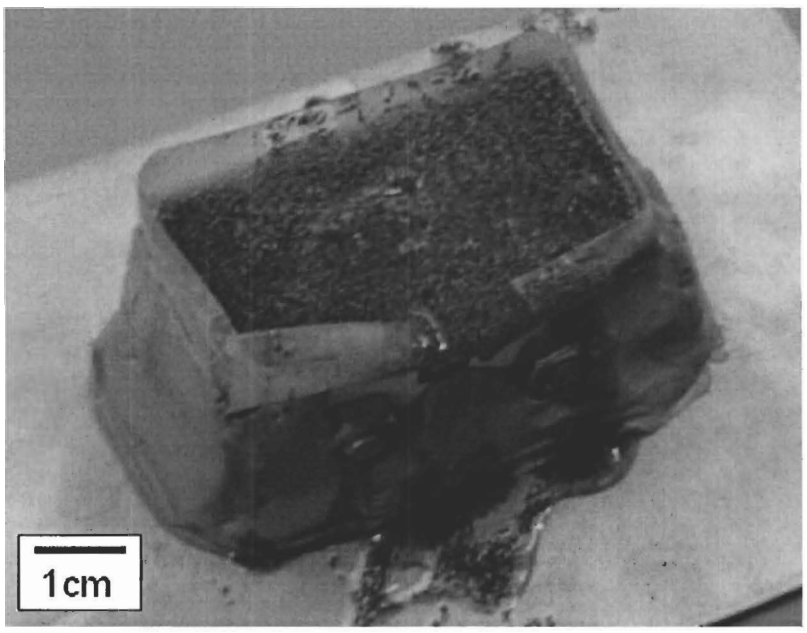

Figure C- 4: MRE in the Mold

As discussed in the thesis, for our experiments, we created two versions of the MRE. For each version the amount of silicone and beads were constant, we only changed whether the silicone was cured in the presence of a magnetic field. The first version of the MRE was created in the absence of a magnetic field. The beads are evenly distributed as shown in Figure C- 5.

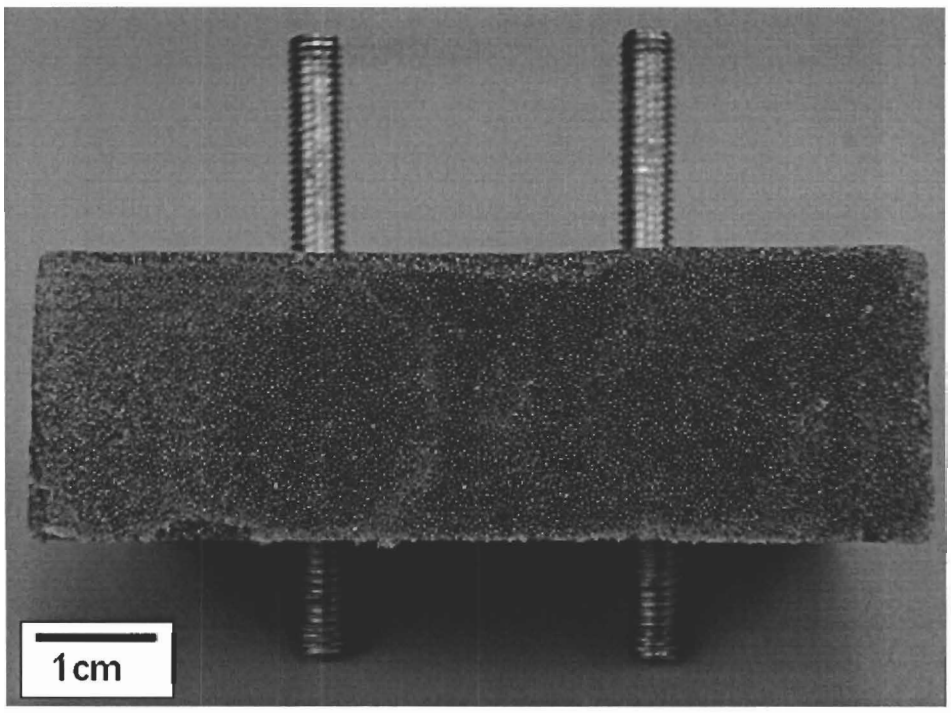

Figure C- 5: MRE Cured with No Magnetic Field

A close up of the iron beads is shown in Figure C- 6.

Figure C- 6: Close-up of Iron Beads When Cured in No Magnetic Field

The second version of the MRE was cured in the presence of a magnetic field. In this case, because the silicone is not cured when the field is applied, the iron beads will

form chain-like structures because of the field lines. Figure C- 7 and Figure C- 8 show the MRE cured in a magnetic field and a close-up of the beads, respectively.

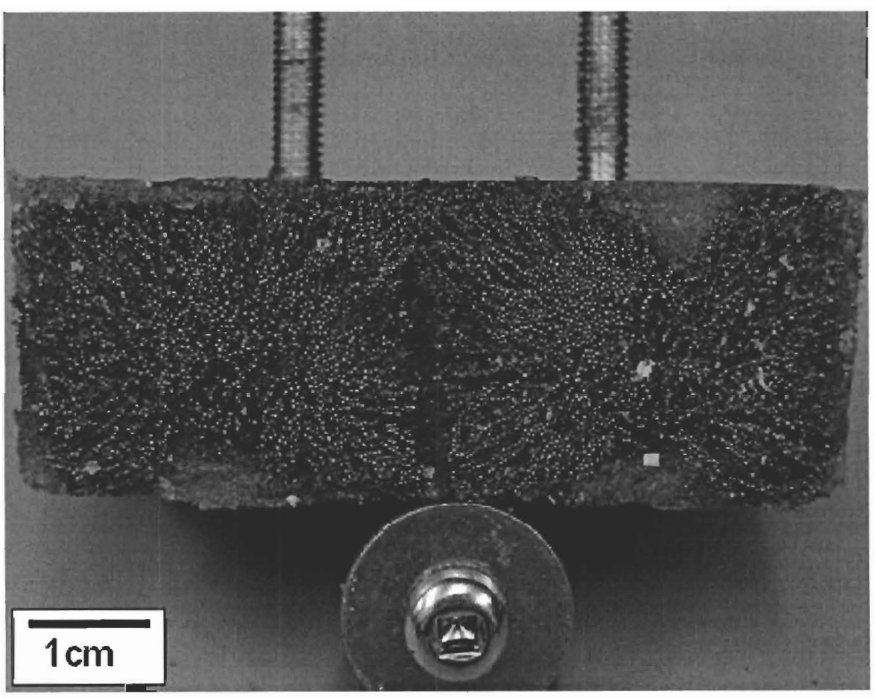

Figure C- 7: MRE Cured in a Magnetic Field

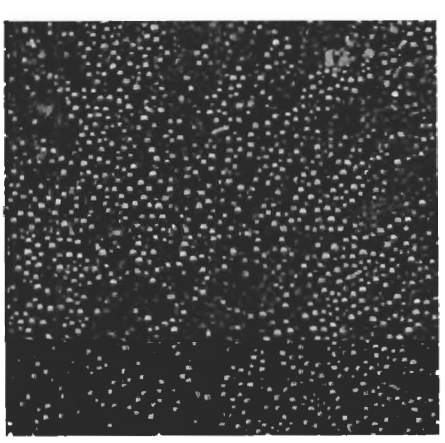

Figure C- 8: Close-up of Iron Beads When Cured in a Magnetic Field

In contrast to the MRE cured without a magnetic field, the beads have now formed a structure in the silicone because of the field lines caused by the magnets.

APPENDIX D:
TEST RIGGING SETUP

The test rigging used for testing the MRE is shown in Figure D- 1.

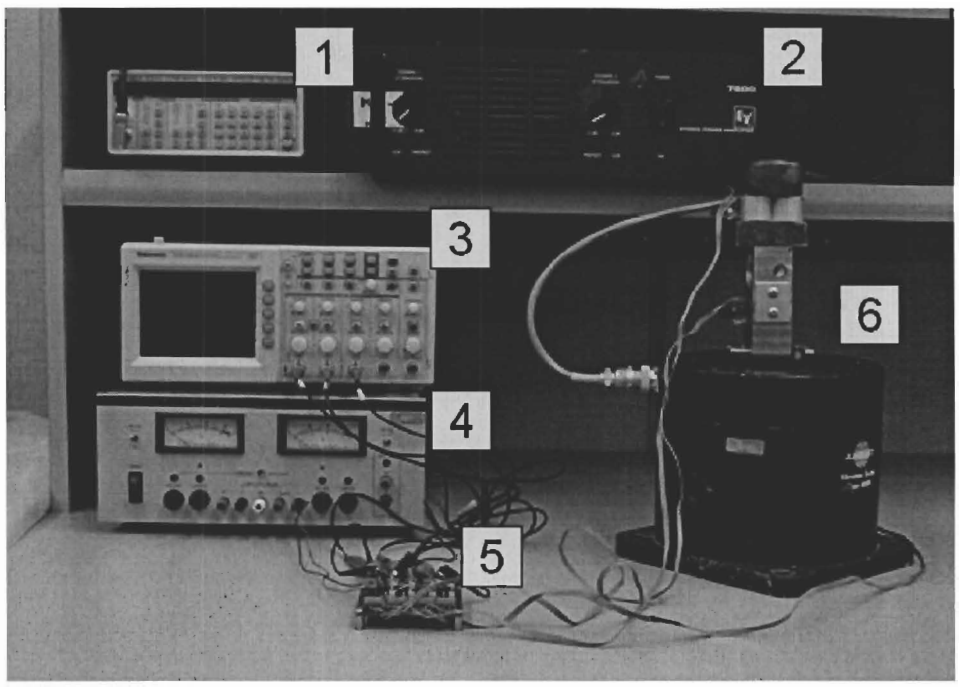

Figure D- 1: Entire Test Rigging Setup

The Table D- 1 summarizes the labeled elements in Figure D- 1.

Table D- 1: Description of Test Rigging Components

Label	Component	Description
1	Function generator	Stanford research systems, model DS345
2	Amplifier	EV stereo power amplifier, model 7600
3	Oscilloscope	Tektronix, TDS 2014
4	Power supply	King Instrument Electronics Co., Ltd. 1353B DC Power Supply
5	Accelerometer buffer board	Designed in-house
6	Shaker table	Bruel & Kjour PM vibration exciter, type 4808

The signal from the function generator is amplified by the amplifier and used to drive the shaker table. The accelerometers are powered by the power supply shown in the figure. The output from the accelerometer is connected to the buffer board (discussed later), which is connected to the oscilloscope. The measurement is set as a 16 sample average. A screen capture from the output is shown in Figure D- 2.

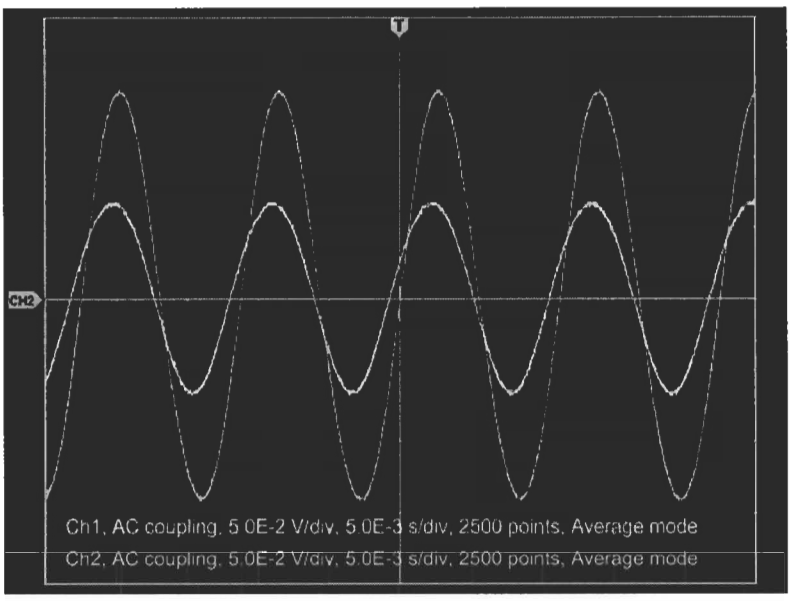

Figure D- 2: Oscilloscope Screen Capture

The transmissibility of the MRE is calculated by dividing the amplitude of the sine wave from accelerometer 2 by the amplitude of the sine wave from accelerometer 1. Figure D- 3 shows a close-up view of the shaker table assembly.

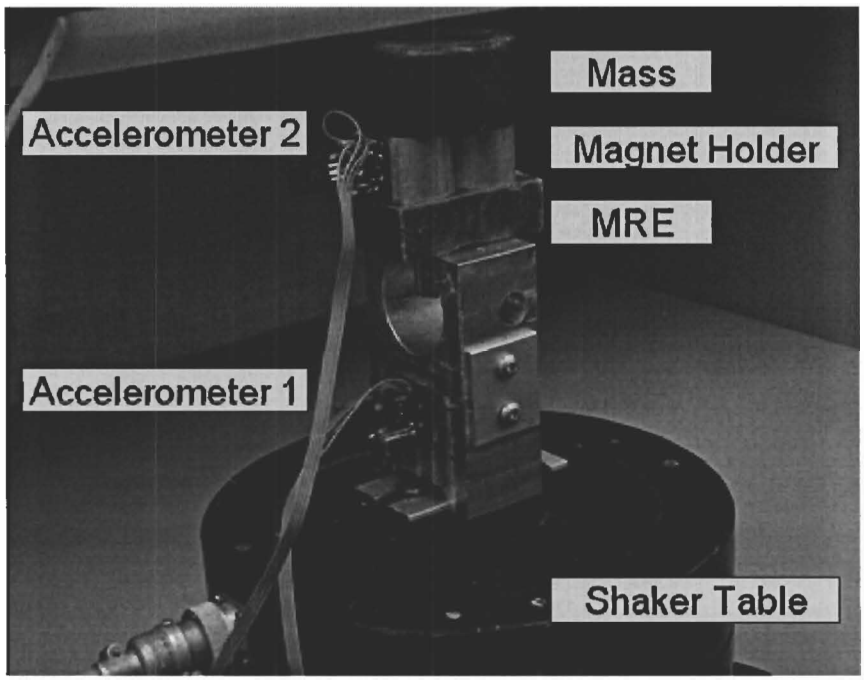

Figure D- 3: Components of the Shaker Table Assembly

In order to test the response of the MRE in a magnetic field, we used two permanent magnets (Lee Valley 99K32.11 3/4''x 1/8'') in a steel cup (Lee Valley 99K32.52) as shown in Figure D- 4.

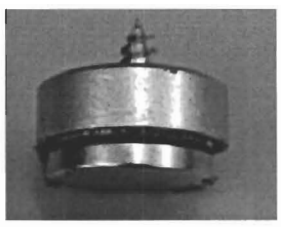

Figure D- 4: Magnets and Steel Cup Used for the Experiments

The screw shown in the figure is used to remove the magnets from the test apparatus. Each of these magnet configurations has a magnetic field strength of 0.258 Tesla 1mm away from the surface. Two of these magnet configurations were placed in the magnet holder shown in Figure D- 5.

Figure D- 5: Magnet Holder

The magnet holder affixed to the MRE with the magnets being placed inside is shown in Figure D- 6.

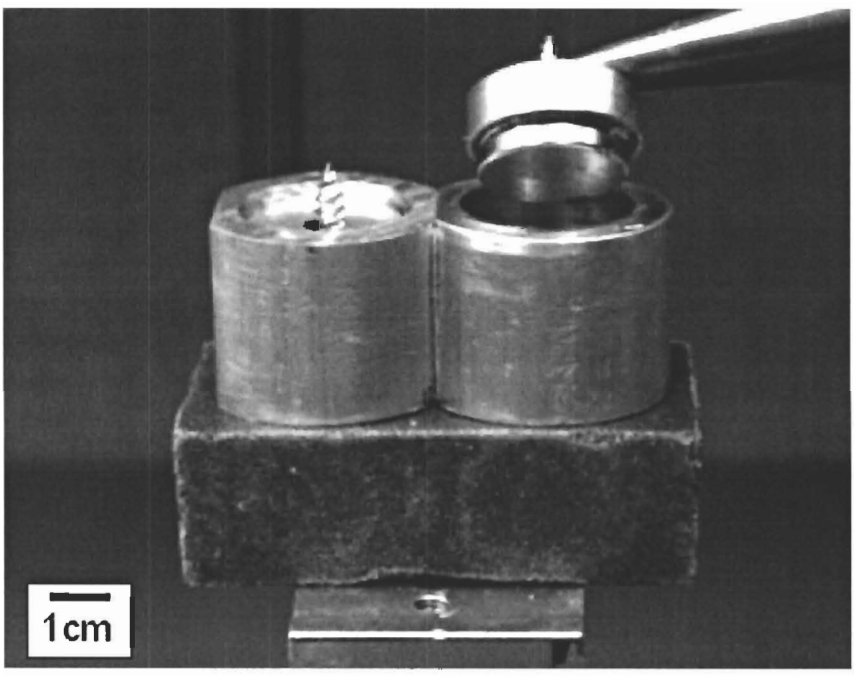

Figure D- 6: Magnets Placed within the Shaker Assembly

For the experiments of the semi-active bushing, we used the X_{out} and Y_{out} pins of the ADXL210 accelerometer (see Appendix B), which gave a modulated signal that needs to be decoded using a microcontroller. For the MRE experiments, we used the X_{filt} and Y_{filt} pins of the accelerometer. These pins give a sinusoidal output whose RMS is the acceleration. We decided to use these output pins because we could measure accelerations at higher frequencies. We discovered with the semi-active bushing experiments that our upper frequency was limited due to the microcontroller.

The X_{filt} and Y_{filt} of the accelerometer need to have their signal buffered in order to work properly. The buffer board we fabricated is shown in Figure D- 7.

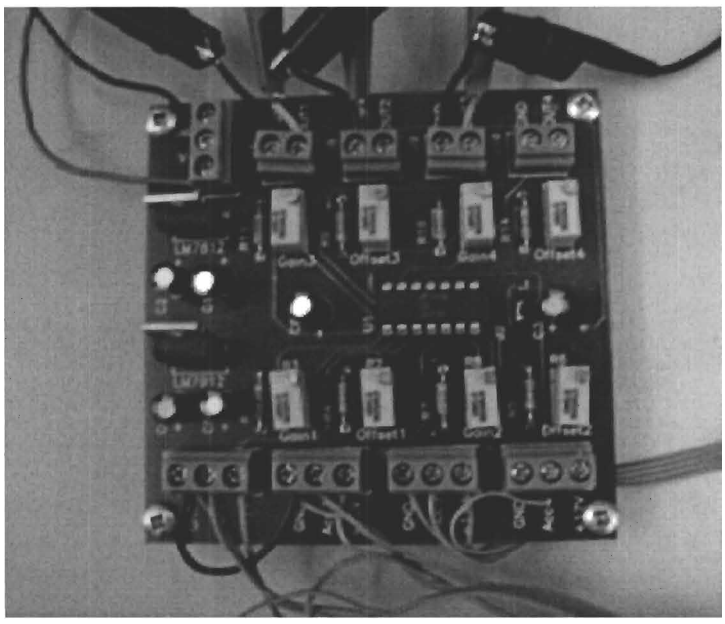

Figure D- 7: Accelerometer Buffer Board

The buffer board's schematic is illustrated in Figure D- 8. The board contains a positive 12 volt regulator and a negative 12 volt regulator. For our current design, we are only using the positive regulator, the negative regulator may be used in subsequent experiments.

The other elements on the PCB are four identical non-inverting amplifiers with a variable offset. The op-amps are set to unity gain with no offset at the positive terminal for our experiments.

Figure D- 8: Buffer Board Schematic

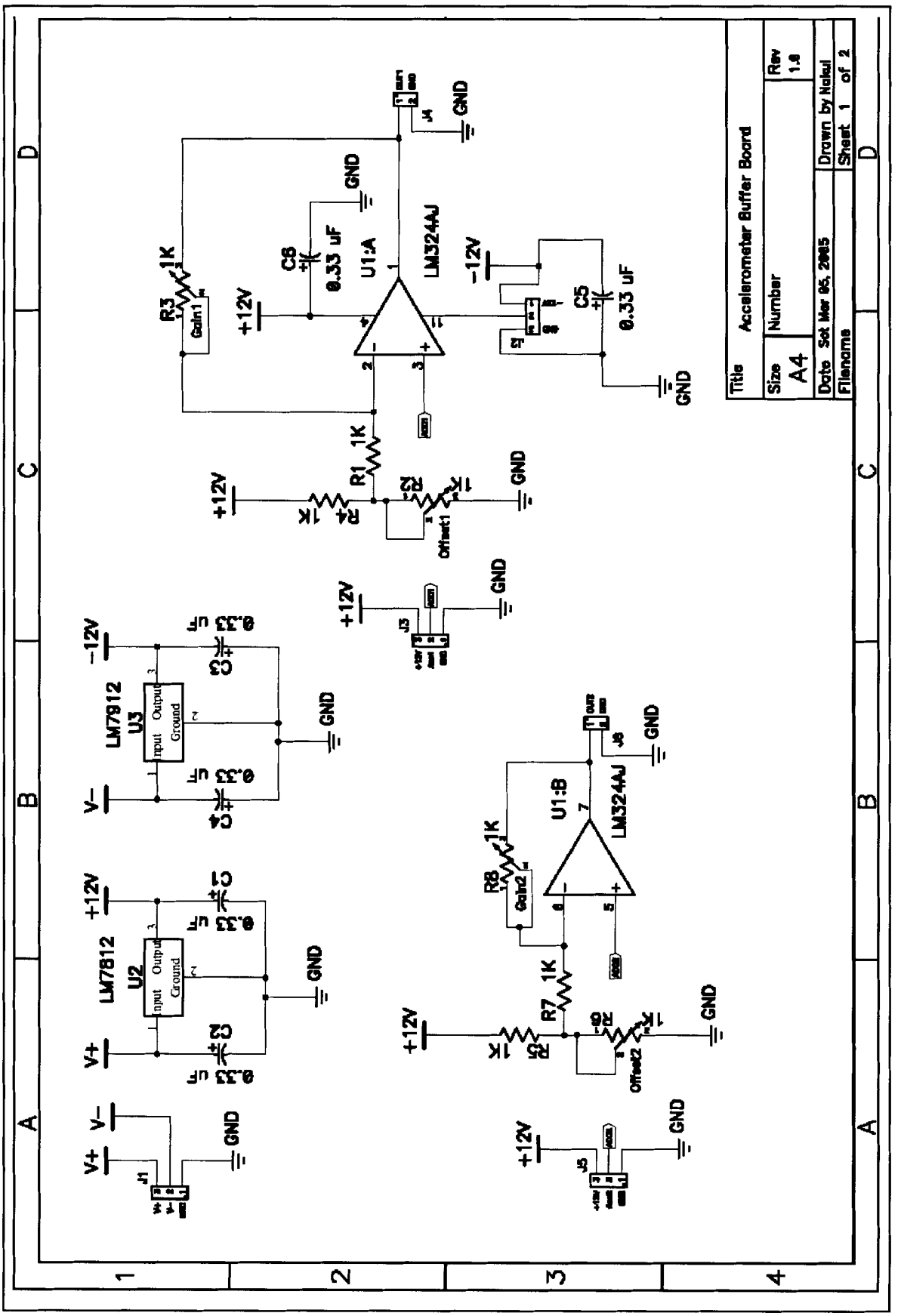
Title Accelerometer Buffer Board
Size A4
Number
Rev 1.0
Date Sat Mar 05, 2005
Drawn by Nakul
Filename
Sheet 1 of 2
LM324AJ
U1:A
U1:B
LM7812
LM7912
Input Output Ground
R1 1K
R2 1K
R3 1K
R4 1K
R5 1K
R7 1K
R8 1K
C1 0.33 uF
C2 0.33 uF
C3 0.33 uF
C4 0.33 uF
C5 0.33 uF
C6 0.33 uF
+12V
-12V
V+
V-
GND
Offset1
Offset2
Gain1
Gain2

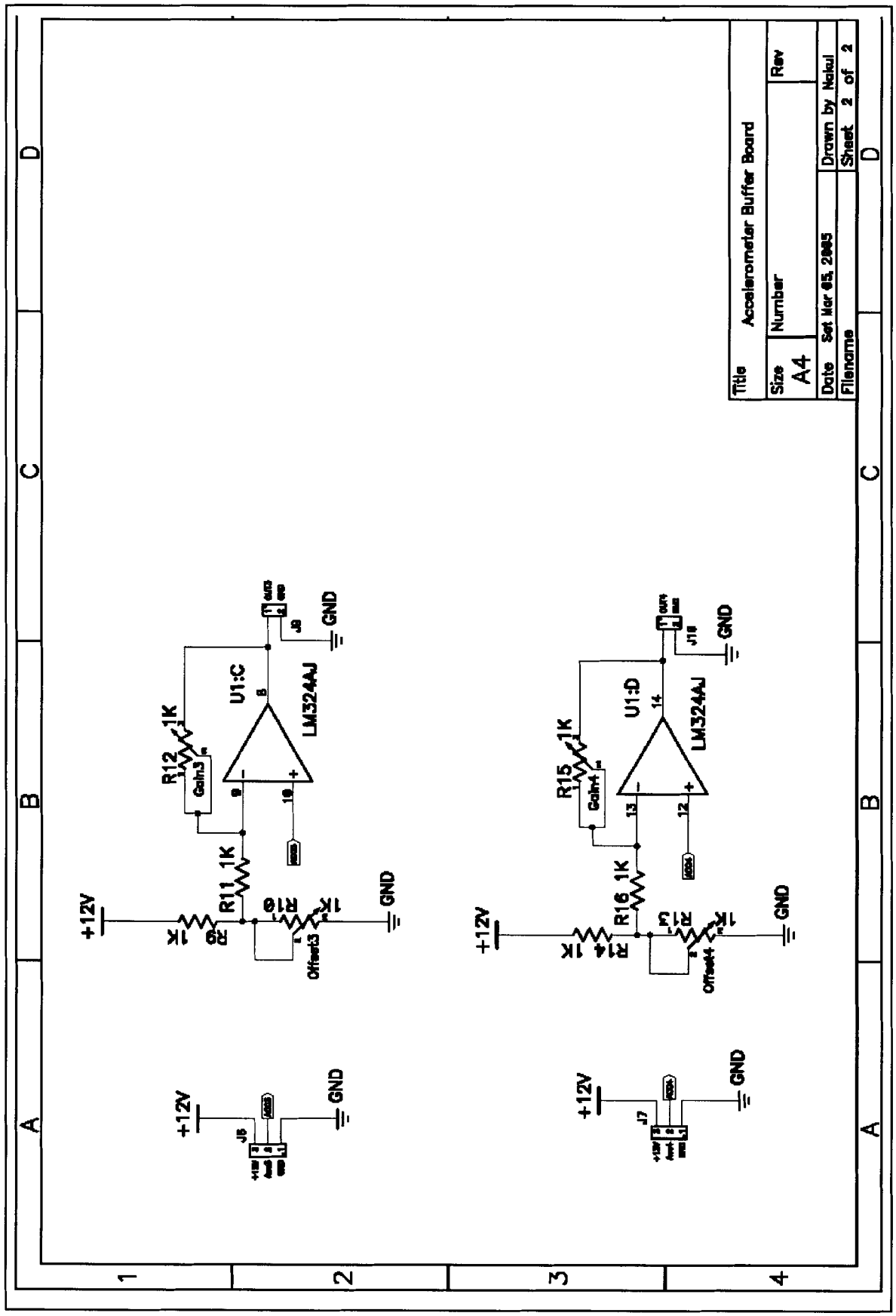
Title Accelerometer Buffer Board
Size A4
Number
Rev
Date Sat Mar 05, 2005
Drawn by Nakul
Filename
Sheet 2 of 2
U1:C
LM324AJ
U1:D
LM324AJ
R11 1K
R12 1K
R15 1K
R16 1K
R9 1K
R10 1K
R13 1K
R14 1K
Gain3
Gain4
Offset3
Offset4
+12V
GND